

8-30-2011

Investigating evidence of high frequency glacial eustacy in the Lower Mississippian (Tournasian) Lodgepole Formation of southwest Montana : insights from conodont oxygen isotopes

Zachary Wallace

Follow this and additional works at: https://digitalrepository.unm.edu/eps_etds

Recommended Citation

Wallace, Zachary. "Investigating evidence of high frequency glacial eustacy in the Lower Mississippian (Tournasian) Lodgepole Formation of southwest Montana : insights from conodont oxygen isotopes." (2011). https://digitalrepository.unm.edu/eps_etds/97

This Thesis is brought to you for free and open access by the Electronic Theses and Dissertations at UNM Digital Repository. It has been accepted for inclusion in Earth and Planetary Sciences ETDs by an authorized administrator of UNM Digital Repository. For more information, please contact disc@unm.edu.

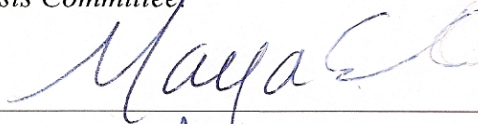
Zachary A. Wallace
Candidate

Earth and Planetary Sciences
Department

This thesis is approved, and it is acceptable in quality
and form for publication:

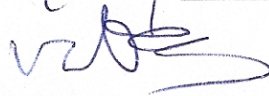
Approved by the Thesis Committee

Dr. Maya Elrick

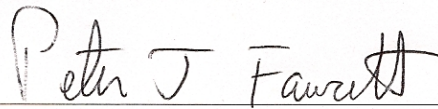


, Chairperson

Dr. Viorel Atudorei



Dr. Peter Fawcett



**INVESTIGATING EVIDENCE OF HIGH FREQUENCY
GLACIAL EUSTASY IN THE LOWER MISSISSIPPIAN
(TOURNAISIAN) LODGEPOLE FORMATION OF
SOUTHWEST MONTANA: INSIGHTS FROM CONODONT
OXYGEN ISOTOPES**

by

ZACHARY ALEXANDER WALLACE

B.S. Geological Sciences, Ohio University, 2008

THESIS

Submitted in Partial Fulfillment of the
Requirements for the Degree of

**MASTER OF SCIENCE IN
EARTH AND PLANETARY SCIENCES**

The University of New Mexico
Albuquerque, New Mexico

July 2011



I want to first thank my advisor Dr. Maya Elrick for her patience. Through her mentoring and guidance I have become a better scientist and more importantly a better man. I am extremely appreciative for the advice and feedback from my committee members Dr. Peter Fawcett and Dr. Viorel Atudorei.

I want to give sincere thanks to V for battling a finicky mass spec in order to run my samples. Also V, your culinary skills, homemade wines, and plum brandy are good enough reasons for me to never leave New Mexico, thank you for your hospitality.

Special thanks to my field assistants the McNamara family, Beth Helmke, Owen Shufeldt, and the hikers of Sacagawea Peak for risking life and limb carrying down ~700 kg of rock off a mountain side. I want to extend gratitude to my lab assistant and good friend, Leilani Ringkvist. Had it not been for her time and effort in the lab, I'd more than likely still be picking conodonts. I am forever grateful...

To my pals, Maarten de Moor, Matt Kirk, and Ryan Crow (hiss!!) thank you for being so efficient in pulling me away from my work time after time with fly fishing trips.

Lastly, to my parents John and Beth, little brother Jake, and aunt Janie you all have sacrificed for the furthering of my education and I am eternally thankful for your encouragement over the last three years. I only hope one day that I can be as supportive to all of you.

**INVESTIGATING EVIDENCE OF HIGH FREQUENCY
GLACIAL EUSTASY IN THE LOWER MISSISSIPPIAN
(TOURNAISIAN) LODGEPOLE FORMATION OF
SOUTHWEST MONTANA: INSIGHTS FROM CONODONT
OXYGEN ISOTOPES**

by

ZACHARY ALEXANDER WALLACE

ABSTRACT OF THESIS

Submitted in Partial Fulfillment of the
Requirements for the Degree of

**MASTER OF SCIENCE IN
EARTH AND PLANETARY SCIENCES**

The University of New Mexico
Albuquerque, New Mexico

July 2011

**INVESTIGATING EVIDENCE OF HIGH FREQUENCY GLACIAL
EUSTASY IN THE LOWER MISSISSIPPIAN (TOURNAISIAN)
LODGEPOLE FORMATION OF SOUTHWEST MONTANA:
INSIGHTS FROM CONODONT OXYGEN ISOTOPES**

ZACHARY ALEXANDER WALLACE

B.S. Geological Sciences, Ohio University, 2008

M.S. Earth and Planetary Sciences, University of New Mexico, 2011

**MASTER OF SCIENCE IN
EARTH AND PLANETARY SCIENCES**

The University of New Mexico
Albuquerque, New Mexico

July 2011

ABSTRACT:

This study focuses on high-frequency (10^4 - 10^5 yr), subtidal-carbonate cycles (1-8 m thick) within the Woodhurst Member of the Lower Mississippian Lodgepole Formation of southwest Montana. We combined conodont-oxygen isotopes ($\delta^{18}\text{O}_{\text{apatite}}$) and carbonate-carbon isotopes ($\delta^{13}\text{C}_{\text{carb}}$) with cyclostratigraphy of Woodhurst cycles to test the hypothesis that the cycles developed in response to glacial eustasy, evaluate the timing of initiation of the Late Paleozoic Ice Age (LPIA), and to better understand the carbon budget in response to cycle formation.

We recognize three scales of depositional cyclicity, approximately 25 (meter scale) cycles stack into 5 intermediate sequences (~15-30 m thick), of which 4 intermediate sequences group into a single full My-scale depositional sequence (~70 m thick).

$\delta^{18}\text{O}_{\text{apatite}}$ values range from 18-21.6 ‰ and fall within the range of previously reported $\delta^{18}\text{O}_{\text{apatite}}$ values from globally dispersed coeval deposits. $\delta^{18}\text{O}_{\text{apatite}}$ trends across targeted cycles support the hypothesis that water depth changes were the result of the waxing and waning of glacial ice combined with cooling surface seawater temperatures (SST). The mean $\delta^{18}\text{O}_{\text{apatite}}$ shift (1.4 ‰) across targeted cycles translate into to ~40-90 m sea-level fluctuations associated with 2-4°C SST changes. Calculated sea-level magnitudes suggest the existence of an ice sheet roughly equal in size to the present day East Antarctic Ice Sheet.

High-resolution $\delta^{13}\text{C}_{\text{carb}}$ analysis of whole-rock limestones within eleven cycles reveal invariant or nonsystematic $\delta^{13}\text{C}_{\text{carb}}$ trends, however, the long-term composite $\delta^{13}\text{C}_{\text{carb}}$ trend confirms the pattern of a major positive excursion reported in previous studies of coeval deposits, values peak at ~ 7.5 ‰ in the upper *S. isosticha* conodont Zone.

TABLE OF CONTENTS

1. INTRODUCTION	1
2. GEOLOGIC SETTING AND STRATIGRAPHIC FRAMEWORK	3
3. METHODOLOGY	7
3.1 <i>FIELD METHODS</i>	7
3.2 <i>LABORATORY METHODS</i>	10
4. RESULTS	11
4.1 <i>FIELD RESULTS</i>	11
4.2 <i>LABORATORY RESULTS</i>	23
5. DISCUSSION	27
5.1 <i>STRATIGRAPHIC CYCLICITY</i>	27
5.2 <i>CYCLE $\delta^{18}\text{O}_{\text{apatite}}$ TRENDS</i>	32
5.3 <i>PALEOCLIMATE INTERPRETATIONS</i>	35
5.4 <i>$\delta^{13}\text{C}_{\text{carb}}$</i>	40
5.5 <i>IMPLICATIONS</i>	45
6. CONCLUSIONS	48
7. APPENDICES	50
7.1 <i>APPENDIX 1 STRATIGRAPHIC COLUMN</i>	50
7.2 <i>APPENDIX 2 $\delta^{13}\text{C}_{\text{carb}}$ VALUES</i>	58
7.3 <i>APPENDIX 3 $\delta^{18}\text{O}_{\text{apatite}}$ VALUES</i>	58
REFERENCES	62

1. INTRODUCTION

Over the last several decades the timing and initial patterns of the Late Paleozoic Ice Age (LPIA) have been the subjects of debate. Traditionally the LPIA was thought to be a single, prolonged event stretching from the Late Mississippian to Middle Permian (Veevers and Powell, 1987); however, Isbell et al. (2003) and Fielding et al. (2008) report periods of widespread glaciation separated by intervals of restricted or a total absence of glaciation throughout the Late Paleozoic. These glacial and nonglacial intervals lasted several million years (My), however, the timing of their onset is subject of debate. Fielding et al. (2008) suggest glacial-nonglacial intervals began in the Late Mississippian, while Isbell et al. (2003) advocate the earliest Mississippian. These two camps are based on the age and distribution of the first Late Paleozoic glacial deposits from South America and Australia.

There are two main lines of evidence that suggest the onset of the LPIA occurred during the Late Mississippian (Serpukhovian); the first is the presence of far-field (ice distal) Late Mississippian Euroamerican cyclothems (or cycles), interpreted to represent glacio-eustatic sea-level changes due to cyclic waxing and waning of Gondwanan glaciers (Horbury, 1989; Read et al., 1995; Smith and Read, 1999, 2000; Wright and Vandstone, 2001; Bishop et al., 2009, 2010). The second is the lack of earlier dated near-field glacial deposits, and the abundance of Late Mississippian aged glacial deposits located across Gondwana (Hambrey and Harland, 1981; Crowell, 1983; Caputo and Crowell, 1985; Veevers and Powell, 1987; Frakes et al., 1992; Gonzalez 2001; Fielding et al., 2008).

Recently, the Early Mississippian (Tournaisian) has been suggested as the stage in which the LPIA began (e.g., Buggisch et al., 2008). Traditionally, the Early Mississippian was considered a greenhouse climate based on the wide-latitude distribution of carbonate and evaporite facies along with a lack of glacial deposits (Frakes et al., 1992). However, there is new evidence to suggest the presence of Tournaisian ice; alpine-glacial deposits across Gondwana and potentially the eastern U.S. (Cecil et al., 2002; Isbell et al., 2003; Brezinski et al., 2008), stacked high-frequency (10^4 - 10^5 yr), carbonate cycles in the Lodgepole Formation of the northern Rocky Mountains interpreted to represent moderate (~20-25 m) sea-level fluctuations (Elrick and Read, 1991), and finally, the Blackhand Sandstone of southeastern Ohio has been inferred as a paleovalley that formed in response to an estimated 60 m glacio-eustatic sea-level fall during the late Tournaisian (Matchen and Kammer, 2006).

Stable isotope data have also been used to support cooling and glaciation during the Early Mississippian. For example, increasing oxygen isotope ratios in brachiopod calcite (Bruckschen and Veizer, 1997; Mii et al., 1999) and conodont apatite (Buggisch et al., 2008), across the Tournaisian are interpreted to represent a combination of cooling and ice buildup. Increasing whole-rock carbonate $\delta^{13}\text{C}$ values from North America and Europe are interpreted to represent an increase in organic carbon (C_{org}) burial resulting in a drawdown of atmospheric CO_2 levels related to enhanced regeneration of phosphate under anoxic conditions in western North America (Mii et al., 1999; Saltzman, 2002; Saltzman et al., 2004).

This debate highlights the difficulties in pinpointing the timing of glacial onset and requires either a more detailed, high-resolution investigation, or indicates that there is not a definitive “onset” but rather a continuum between greenhouse and icehouse climates.

In this study we test the hypothesis that meter-scale, subtidal cycles within the lower Mississippian Lodgepole formation of southwest Montana are the product of high-frequency (30-110 ky) glacial eustasy. To test this hypothesis, this paper 1) describes the distribution of facies in subtidal cycles; 2) evaluates the origins of cycles and magnitudes of climate change using oxygen isotopes derived from conodont apatite ($\delta^{18}\text{O}_{\text{apatite}}$); and 3) discusses the timing of the onset of the LPIA.

2. GEOLOGIC SETTING AND STRATIGRAPHIC FRAMEWORK

The Mississippian represents a time of continental amalgamation prior to the full formation of the supercontinent Pangaea. During this time, North America and Europe were joined as one landmass (Euroamerica) that straddled the paleoequator, while Gondwana was located in the Southern Hemisphere with large areas that covered low to polar latitudes (Fig. 1A).

During the Early Mississippian, the western edge of North America was characterized by a westward-dipping, distally-steepened, carbonate ramp stretching from the southwest U.S. to northern Canada (>700 km wide, 1600 km long) (Sando 1976; Poole and Sandberg 1977). East of the ramp lay the partially submerged Transcontinental Arch with the Antler Orogenic Highlands and the

Antler Foreland Basin to the west, while Montana was located $\sim 5\text{-}10^\circ$ north of the paleoequator (Fig. 1B) (Blakey, 2011). The Late Devonian-Early Mississippian Antler convergent event emplaced an extensive allochthon of oceanic sediment onto the continental shelf, produced subsidence of an elongate foreland basin, and preserved highlands in the interior region of the allochthon during and after the subsidence of the foreland basin (Speed and Sleep, 1982).

We examined the deeper subtidal-ramp deposits of the Lower Mississippian (Tournaisian) Woodhurst Member of the Lodgepole Formation in southwestern Montana. The study area is located ~ 40 miles north of Bozeman, MT in the Bridger Range near Sacagawea Peak. Here, the Lodgepole Formation is ~ 225 m thick while the coeval Lower Madison Formation thins to ~ 20 m in eastern Wyoming.

The Lodgepole Formation is divided into three members, in ascending order, the Cottonwood Canyon, Paine, and Woodhurst Members (Fig. 2). The basal Cottonwood Canyon Member, composed of siliciclastics, unconformably overlies a major Late Devonian/Early Mississippian unconformity, the Paine Member is characterized by deep-water carbonate and mud mound deposits, while the overlying Woodhurst Member represents a transition from deep to shallow-water carbonate deposition, and is conformably overlain by the mid-Mississippian Mission Canyon Formation (Fig. 2). The age of the Lodgepole Formation is mid Tournaisian based on foraminifera and conodont biostratigraphy (Gutschick et al., 1980; Sando, 1985).

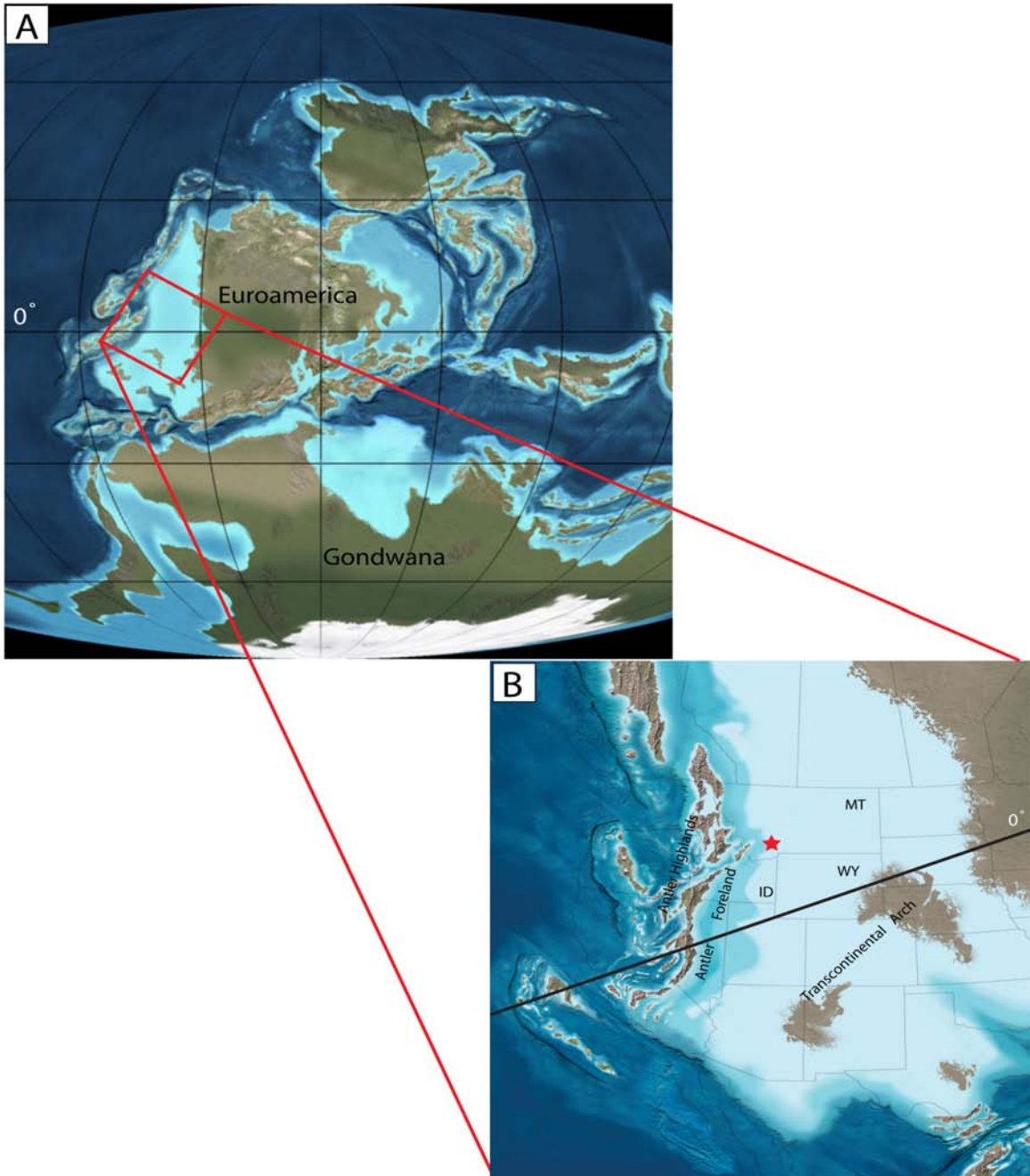


Figure 1: Early Mississippian (Tournaisian ~ 350 Ma) paleogeography, after Blakey, (2011). **(A)** Global paleogeographic map of Euroamerica straddling the paleoequator and Gondwana stretching from subtropical to polar latitudes. **(B)** Western N. American paleogeography of a westward dipping distally steepened carbonate ramp from New Mexico into Canada, east of the ramp is the partially submerged Transcontinental Arch, west of the ramp are the Antler Highlands and Foreland Basin. The red star indicates outcrop locality ~ 5-10 °N of the paleoequator.

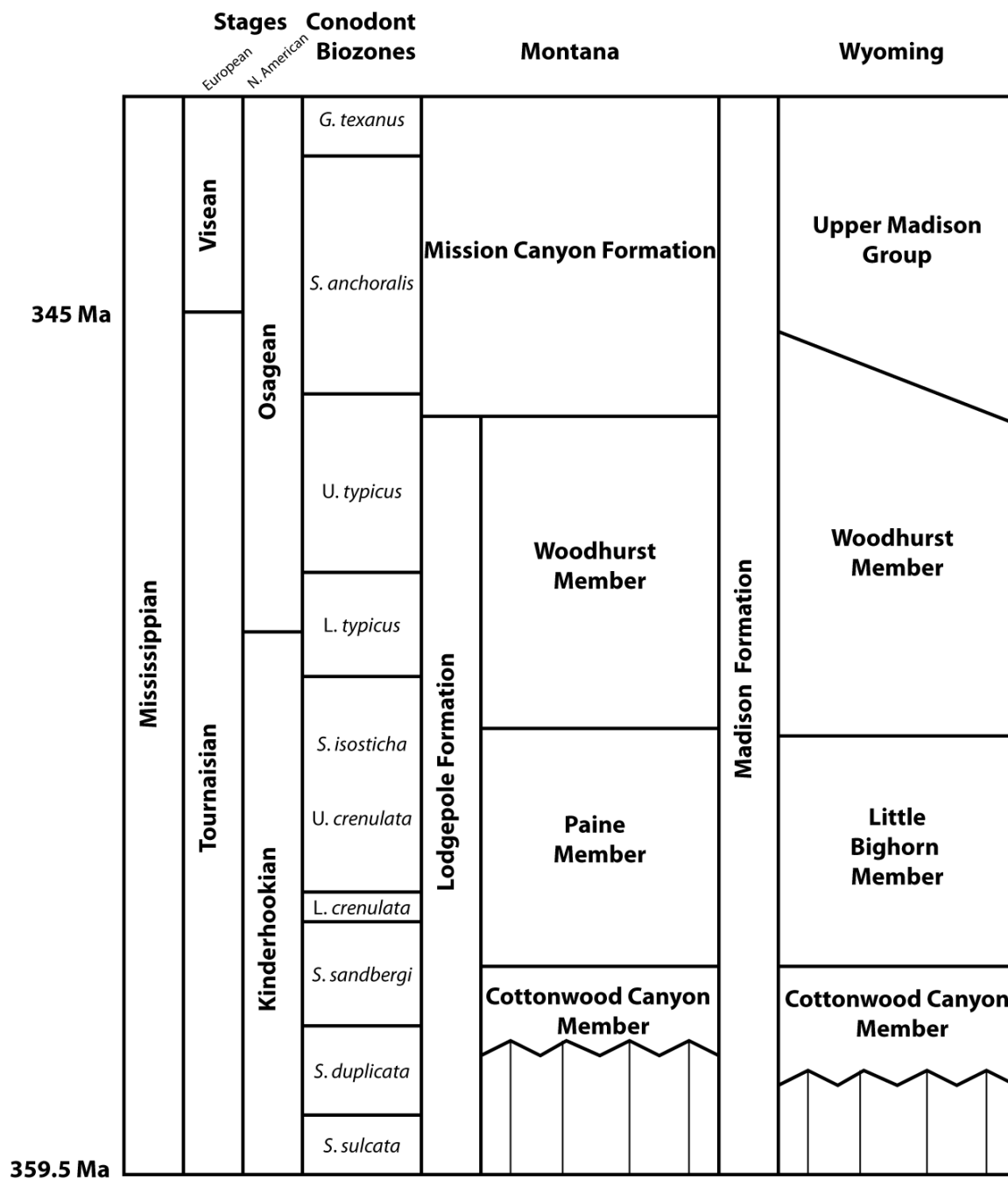


Figure 2: Chronostratigraphic chart of Lower Mississippian stratigraphy of Montana and Wyoming. Timescale from Gradstein et al. (2004).

Previous researchers examining the Lodgepole and coeval Madison Formations described three correlative My-scale depositional sequences (70-100 m thick) across the Lower Mississippian platform in Montana, Wyoming, and Idaho (Elrick and Read, 1991; Sonnenfeld, 1996; Katz et al., 2007), which can be further correlated with three Tournaisian My-scale depositional sequences in the Mississippi Valley (midcontinent USA), the Russian Platform, and northwest Europe (Ross and Ross, 1985). In southwest Montana, My-scale depositional sequences are comprised of several intermediate sequences (~15-30 m thick), which are composed of stacked meter-scale high-frequency (10^4 - 10^5 year) subtidal cycles (Fig. 3A & 3B).

3. METHODOLOGY

3.1 FIELD METHODS

We focused on ~ 90 m of the Woodhurst Member (140 m thick) at the study area (Fig. 4). This portion of the Woodhurst Member was targeted because it contains high-frequency subtidal cycles, and facies within cycles are suitable for conodont preservation. The Paine Member does not contain subtidal cycles and the basal Cottonwood Canyon Member is siliciclastic dominant so these members were avoided.

The lower to lower-upper Woodhurst section was measured bed-by-bed, describing lithologies, fossil assemblages, sedimentary structures, bed thickness, and geometries in order to define facies and interpret depositional environments

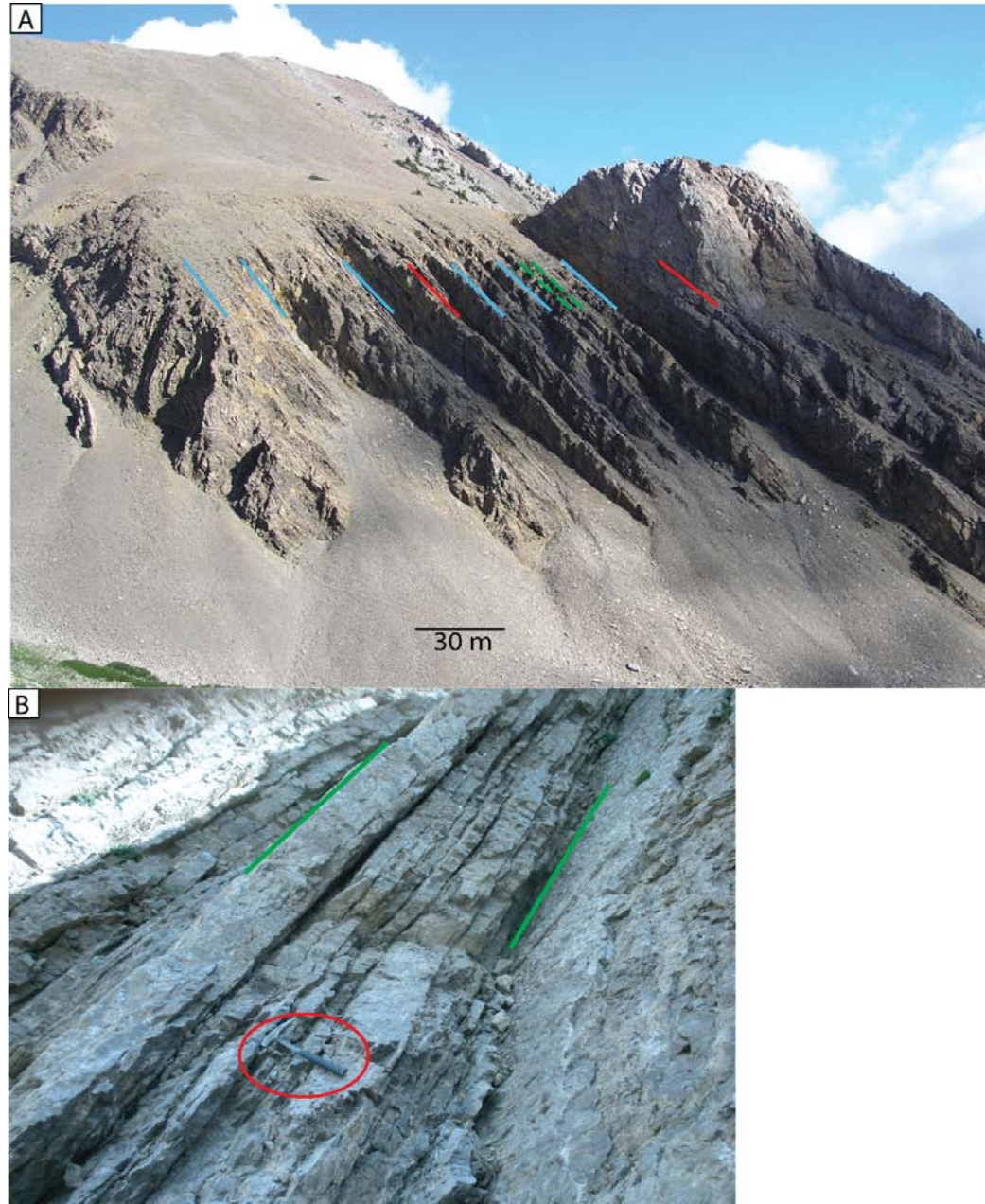


Figure 3: Outcrop photos **(A)** Field photograph of a portion of the Lodgepole Formation (Paine and Woodhurst Members) in study are showing 3 scales of cyclicity: red lines indicate My-scale depositional sequence boundaries, blue lines outline intermediate sequences, and green lines outline cycle boundaries. **(B)** Field photograph of a complete meter-scale cycle composed of rhythmic facies abruptly overlain by a thick crinoidal-grainstone cap. Green lines outline cycle boundaries.

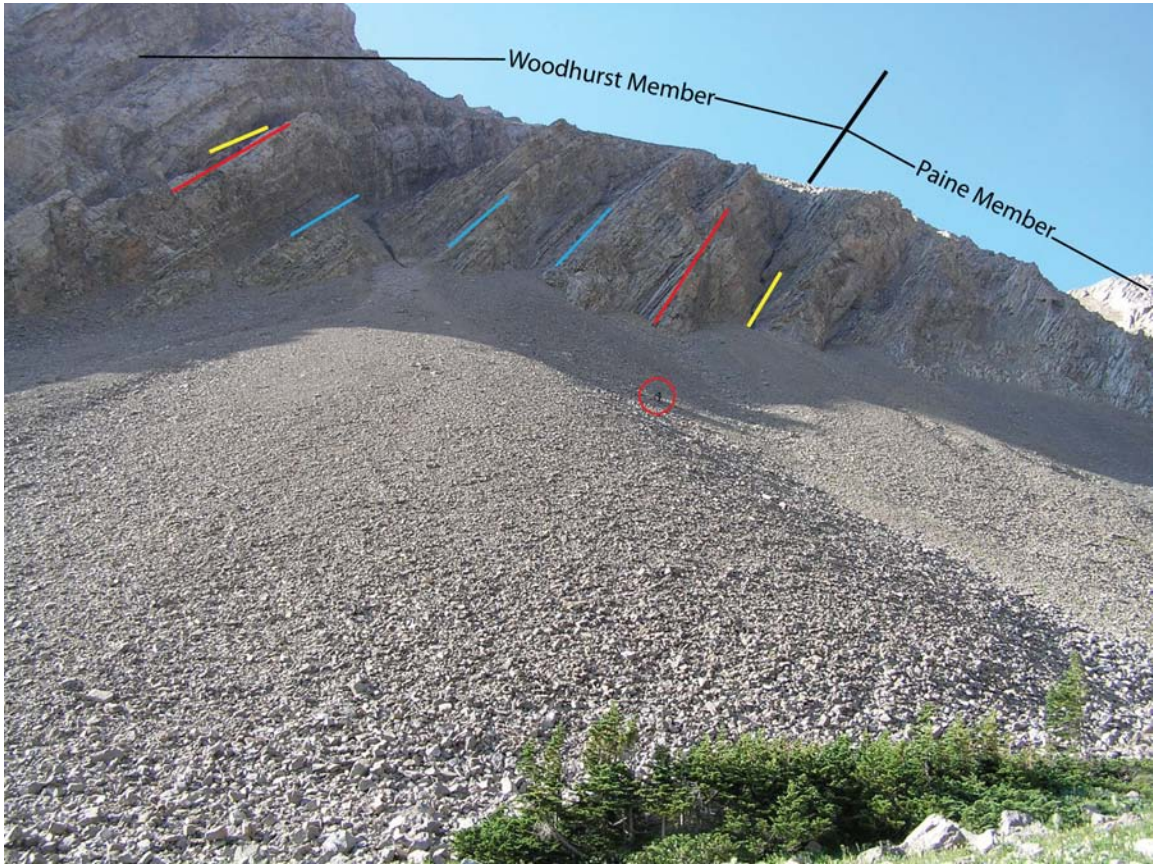


Figure 4: Outcrop photograph of a portion of the Lodgepole Formation ~40 miles North of Bozeman, MT in the Bridger Range near Sacagawea Peak. Red and blue lines are equivalent to Figure 3. Yellow lines indicate boundaries of measured section. Red circle surrounds primary author. This outcrop is accessed via the Sacagawea Peak trailhead near Fairy Lake.

(Table 1). The vertical pattern of facies changes defined ~ 25 cycles. Once cycles were defined, conodont samples (3-10 kg) were collected within a cyclostratigraphic framework (roughly at 0.5 m intervals). A total of 49 samples were collected from eleven cycles, of which 20 produced enough conodonts over five cycles for analysis.

Also, whole-rock carbonate carbon ($\delta^{13}\text{C}_{\text{carb}}$) samples (90 +) were collected at 0.20 to 0.5 m intervals within 11 cycles to determine if systematic $\delta^{13}\text{C}_{\text{carb}}$ trends developed across Lower Mississippian cycles similar to those reported in Pleistocene glacial-interglacial cycles (e.g., Ruddiman, 2008).

3.2 LABORATORY METHODS

Conodont samples were processed using standard concentration techniques developed by Sweet and Harris (1989). Once concentrated, conodont apatite was converted to Ag_3PO_4 using a modified method derived from O'Neil et al. (1994), ensuring that only phosphorus-bound oxygen was analyzed (detailed description of the Ag_3PO_4 conversion can be found in Elrick et al., 2009). $\delta^{18}\text{O}_{\text{apatite}}$ values were obtained by measuring the Ag_3PO_4 crystals by continuous flow TC-EA isotope ratio mass spectrometry using a ThermoFinnigan TC-EA coupled to a Finnigan Mat 252 Mass Spectrometer via a CONFLO III Interface in the Stable Isotope Laboratory, Department of Earth and Planetary Sciences, University of New Mexico. We report values against laboratory standards (ACROS-2 13.5 ‰, MS 22.39 ‰, WT 19.87 ‰) and an international standard TU-1 21.11 ‰ (Venneman et al., 2002). We also measured NBS-120c for which we obtained a $\delta^{18}\text{O}$ value of 22.6 ‰. The uncertainty, based on long-term measurement of phosphate standards, is <0.3 ‰ and is overseen by multiple-standard analyses interspersed with samples. Values are reported relative to Standard Mean Ocean Water (SMOW).

Prior to Ag_3PO_4 conversion, select conodonts were photographed under a binocular microscope to determine a conodont alteration index (CAI). Once photographed, conodonts were imaged using Scanning Electron Microscopy (SEM).

Whole-rock carbonate samples were measured for $\delta^{13}\text{C}$ and $\delta^{18}\text{O}$ values in the Stable Isotope Laboratory in the Department of Earth and Planetary Sciences at the University of New Mexico using the method described by Spotl and Vennemann (2003). The samples were loaded in 12 mL borosilicate exetainers, then the exetainers were flushed with He and the samples were reacted for 24 hours with H_3PO_4 at 50 °C. The evolved CO_2 was measured by continuous flow Isotope Ratio Mass Spectrometry using a Gasbench device coupled to a Finnigan Mat Delta Plus Isotope Ratio Mass Spectrometer. The results are reported using the delta notation, versus PDB. Reproducibility was better than 0.15 ‰ for both $\delta^{13}\text{C}$ and $\delta^{18}\text{O}$ based on repeats of a laboratory standard (Carrara Marble). The standards were calibrated versus NBS 19, for which the $\delta^{13}\text{C}$ is 1.95 ‰ and $\delta^{18}\text{O}$ is 2.2 ‰.

4. RESULTS

4.1 FIELD RESULTS

We recognize five major facies in the ~ 90 m thick studied Woodhurst interval located ~ 40 miles North of Bozeman, MT in the Bridger Range near Sacagawea Peak. Lithologic descriptions are listed in Table 1 with depositional interpretations discussed below.

4.1.1 CRINOIDAL PACK/GRAINSTONE FACIES

Poorly sorted crinoid pack/grainstones (Table 1) contain mud rip-up clasts (Fig. 5A), rare-mega ripples, and occasionally channel-shaped geometries suggesting deposition occurred in higher energy settings between storm and fair-weather wave base (Fig. 6). We interpret the crinoidal pack/grainstones to represent proximal storm deposits along the upper-lower shoreface. Elrick and Read (1991) propose that each pack/grainstone bed represents multiple storm deposits during a period of relatively low sea level rather than the results of a single storm. Paleoflow directions, taken from crest orientations of mega ripples, suggest east-west paleoflow direction. Similar facies interpretations have been reported by Aigner (1985), Osleger and Read (1991), and Soreghan and Giles (1999).

4.1.2 RHYTHMITE FACIES

Thin rhythmically interbedded limestone-marl facies ("rhythmites"-Fig. 5B) (Table 1) occur within the most basinward stratigraphic sections of Elrick and Read (1991) and near the base and middle of cycles and are interpreted here to represent a poorly oxygenated, quiet-water, depositional environment, below storm-wave base (SWB-Fig. 6) based on presence of fine-grain size, suspension laminations, and a lack of wave/current generated features and rare macrofossils. Carbonate layers are typically depleted in fossils but exhibit a massive texture indicative of bioturbation with some suspension laminations

preserved. Marl layers are slightly more fossiliferous, typically massive with occasional suspension laminations preserved. Fossils and sedimentary structures preserved in both the marl and limestone units indicate variable-to dysoxic-bottom waters. Where preserved, limestone and marl layers contain 10's-100's of mm-thick laminae, with each laminae representing deposition from suspension settling from a single distal storm event or turbidity current. A single limestone or marl bed represents many 10's-100's storm events or turbidity currents. Similar sub-storm wave base rhythmites are reported by Cook and Taylor (1977), Read (1980), Handford (1986), Elrick and Snider (2002), and Elrick and Hinnov (2007).

4.1.3 GRADED RHYTHMITE FACIES

Thin rhythmically interbedded-graded limestones and marl ("graded rhythmites") contain millimeter-thick suspension laminae, symmetrical ripples (Fig. 5C) fining-upward lenses/layers on mm-cm-decimeter scales (Fig. 5D), marl drapes, and micro-scour structures, suggesting deposition in storm-dominated environments of the distal-lower shoreface (at or above storm-wave base; Fig. 6). Minimal evidence of bioturbation in both the marl and limestone suggests dysoxic bottom-water conditions. Similar facies interpretations have been suggested by Cook and Taylor (1977), Aigner (1985), and Mohseni & Al-Aasm (2004) for the Cambrian, Triassic, and Paleogene deposits respectively.

The origin of rhythmically interbedded limestone and marl layers is not well understood, but has been attributed to: 1) continuous influx of fine

siliciclastics interrupted by turbidity currents carrying storm-derived detrital carbonates; 2) relatively continuous carbonate storm deposition punctuated by an increase in fluvial derived siliciclastic material; or 3) both periods of carbonate storm deposition alternating with periods of increased siliciclastic influx. For each scenario, wetter to drier paleoclimate fluctuations likely controlled the amount and composition of material transported offshore (Elrick et al., 1991; Elrick and Hinnov, 1996; Elrick and Hinnov, 2007). An increase in siliciclastic material corresponds to wetter paleoclimate conditions, whereas an increase in carbonate material was resultant from more arid paleoclimate conditions.

4.1.4 PELOIDAL GRAINSTONE FACIES

Well-sorted peloidal grainstones exhibit planar laminae (Fig. 5E & F), low angle cross bedding, mud rip-up clasts, and a normal marine fossil assemblage indicating deposition in a high energy, well oxygenated setting (Table 1). This facies is typically restricted to a cycle cap facies. We interpret this facies formed above fair-weather wave base along the upper shoreface (Fig. 6).

4.1.5 OOID GRAINSTONE FACIES

The ooid grainstone facies is interpreted to represent ooid-shoal deposition based on the presence of well-sorted ooids (5G), high-angled cross bedding (Fig. 5H), and rounded-oolitic intraclasts (Table 1). Rounded-oolitic intraclasts and a lack of subaerial exposure features indicate early marine cementation and continuous submergence. Paleoflow was derived from the

high-angled cross bedding indicating flow direction to the south. Throughout the Paleozoic, analogous facies have been reported (e.g. Osleger and Read, 1991; Goldhammer et al., 1993; Huneke et al., 2001). Modern ooids are precipitated in the Bahamas (Lloyd et al., 1987; Tucker and Wright, 1990), the southern Persian Gulf (Loreau and Purser, 1973), and in Shark Bay, western Australia (Hagan and Logan, 1974) in water less than 5 m deep. We suggest similar water depths for Woodhurst ooids.

Facies Name	Lithology and Thickness	Sedimentary Structures	Biota	Cycle Position and Facies Interval Thickness	Depositional Environment Interpretation
Rhythmically Interbedded Limestone and Marl “rhythmites”	Limestone: lime mudstone-skeletal wackestone (0.05-0.2 m thick) Marl: argillaceous-lime mudstone-argillaceous-skeletal wackestone (0.01-0.1 m thick)	Limestone: rare Laminae Marl: mm-thick suspension laminae	Limestone: sparse crinoids, rugose coral (in life position), fenestrate bryozoa, and brachiopods Marl: crinoids, rugose coral, fenestrate bryozoa, brachiopods, vertical and horizontal burrows	Located within the basal/transgressive portion of cycles (0.1-5.0 m thick)	Basin/slope with fluctuating or low oxygen levels below storm wave base
Rhythmically Interbedded Graded Limestone and Marl “graded rhythmites”	Limestone: lime mudstone-skeletal pack/grainstone (0.05-0.2 m thick) Marl: Lime mudstone-skeletal wackestone (0.01-0.1 m thick)	Limestone: fining-upward layers and lenses (mm, cm, decimeter scales), symmetrical ripples, mud drapes, and micro scours Marl: mm-thick parallel laminae and symmetrical ripples	Limestone: fragments of: crinoids, brachiopods, rugose coral, and fenestrate bryozoa Marl: skeletal fragments of: crinoids, brachiopods, and fenestrate bryozoa Zoophycus Chondrites, and both horizontal and	Located within the basal/transgressive portion of cycles (0.1-20.0 m thick)	Lower shoreface with low to moderate oxygen levels near storm wave base.

			vertical borrows		
Crinoidal Pack/Grainstone	Poorly-sorted, coarse, crinoidal pack-grainstone (0.2-0.3 m)	Mud rip-up clasts, planar laminae, rare symmetric mega-rippled tops, and occasionally channel shaped beds.	Crinoids, brachiopods, rugose coral, and fragments of fenestrate bryozoans	Typically forms cycle caps, but can occur near cycle base (when a "shallower" facies peloidal/oid grainstone caps a cycle) (0.2-1.1 m thick)	Upper-lower shoreface (proximal storm deposit)
Peloidal Grainstone	Well-sorted peloidal grainstone (0.2-0.3 m)	Planar and swaly laminae, graded beds, and mud rip-up clasts.	Crinoids, brachiopods, and rugose coral	Restricted to cycle caps (0.1-0.6 m thick)	Upper shoreface
Ooid Grainstone	Well-sorted oolitic grainstone (0.2-.35 m)	Planar laminae, cross bedding, and mud/oolitic rip-up clasts	Skeletal fragments of crinoids, brachiopods, and rugose corals	Restricted to cycle caps (0.2-8 m thick)	Upper shoreface

Table 1: Facies descriptions and depositional environment interpretations

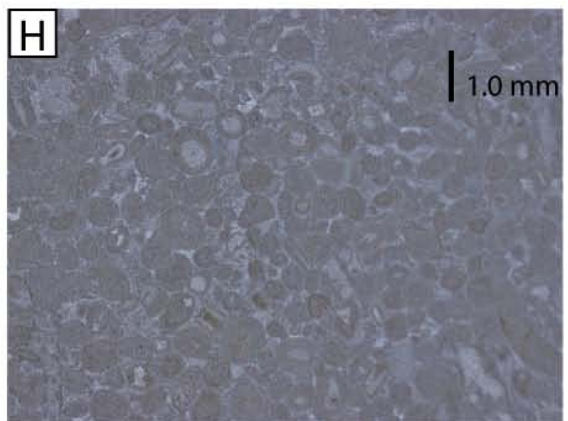
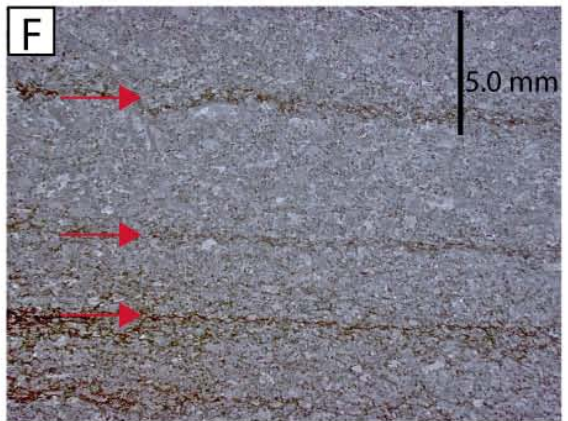
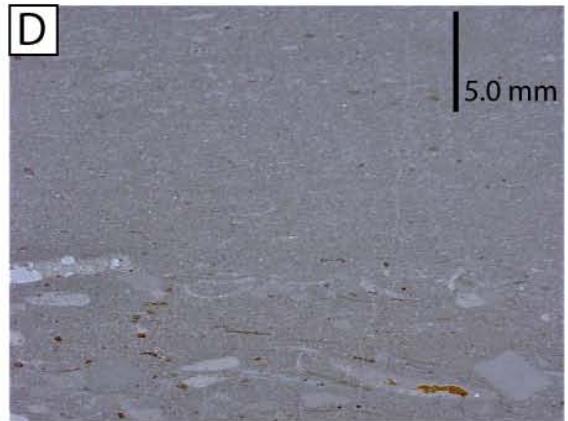


Figure 5: Outcrop and thin section photos of Woodhurst Member facies. **(A)** Coarse-grained crinoidal-grainstone cap with mud rip-up clasts (red arrows) **(B)** Rhythmically bedded lime mudstones (dark gray) and marl (tan) “rhythmites”. **(C)** Limestone layer from graded rhythmite facies, arrow indicating symmetrical ripple. **(D)** Thin section photograph of a mm-scale graded interval (composed of skeletal fragments) within graded rhythmite facies. **(E)** Laminated-peloidal grainstone facies (bed tilted vertical; laminations are difficult to see but are parallel to subparallel to primary author’s finger). **(F)** Thin section photograph of plane laminations (red arrows) within the peloidal grainstone facies. **(G)** Crossbedded-oolitic grainstone cap of a shoal-capped cycle (upper SP section). **(H)** Thin section photograph of ooid grainstone facies.

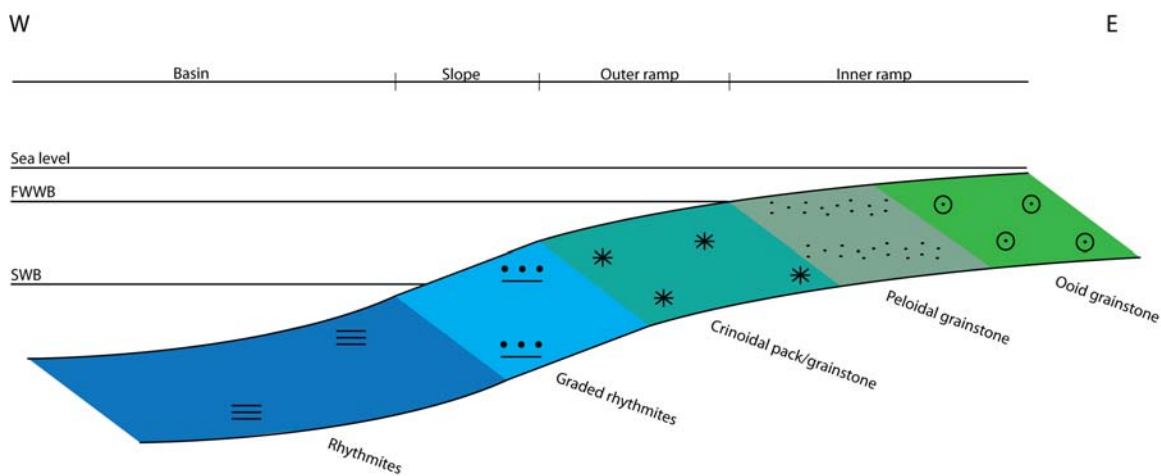


Figure 6: Schematic depositional profile across outer portion of the distally steepened ramp. Peritidal facies lie further east. (see figure 7 for symbol and color explanations).

4.1.6 STRATIGRAPHIC CYCLICITY

4.1.6.1 HIGH-FREQUENCY CYCLES

The 22 stacked subtidal cycles (1-8 m thick) measured within the Woodhurst are composed of substorm wave base through upper shoreface deposits and stack into intermediate and My-scale depositional sequences (Fig. 7). Elrick and Read (1991) estimated average cycle durations of ~ 30-110 ky, by dividing the calculated time range of a biostratigraphically controlled interval by the number of subtidal cycles observed within that controlled interval. Subtidal cycles were used to minimize the effect of time loss and to ensure the full record of sea-level rise, fall, and lowstand (i.e., no exposure surfaces).

Two patterns of subtidal cycles are observed (Fig. 8), regressive (upward-shallowing) and transgressive-regressive (upward deepening then shallowing) cycles. Regressive cycles are typically composed of, in ascending order, lower shoreface graded rhythmite abruptly overlain by upper shoreface crinoidal-peloidal-oolitic pack/grainstones. Transgressive-regressive cycles are composed of, in ascending order, lower shoreface graded rhythmite facies, offshore rhythmite facies, lower shoreface graded rhythmite facies, then capped by upper shoreface pack/grainstones. Both cycle types are capped by either skeletal-rich pack/grainstones (proximal storm capped cycles-PSC) or by upper shoreface ooid-peloid grainstones, shoal deposits (shoal capped cycles-SC). Throughout the measured section, PSC cycles are more abundant and occur within all systems tracts of My-scale depositional sequences. SC cycles occur within all systems tracts (lowstand systems tracts-LST, transgressive systems tracts-TST,

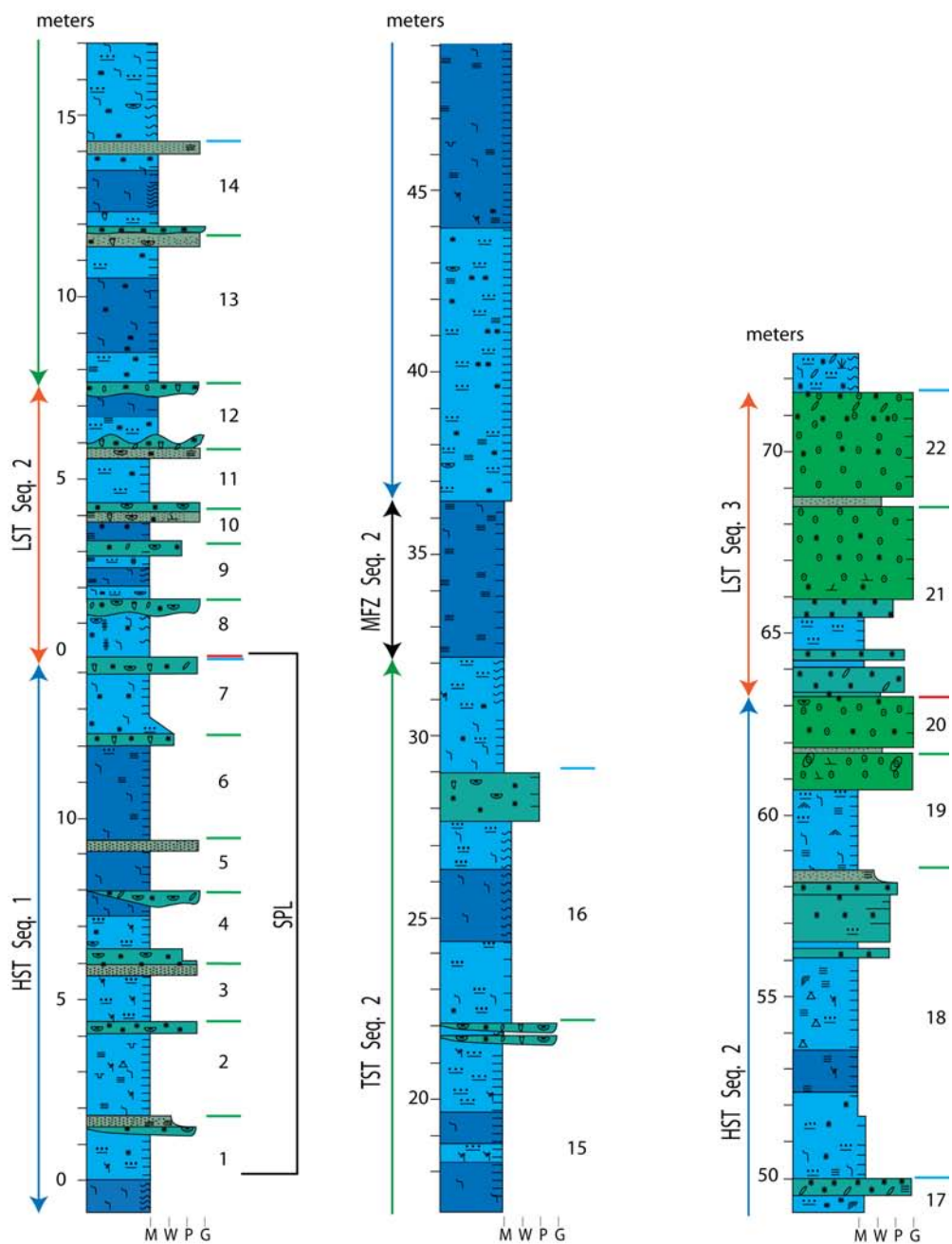
maximum flooding zone-MFZ, highstands systems tracts-HST), however, are most prominent in the LST and late HST of sequences (see Fig. 7). SC cycles provide the best evidence for high-amplitude sea-level fluctuations because substorm wave base rhythmites are abruptly overlain by upper shoreface ooid-peloid grainstones.

4.1.6.2 INTERMEDIATE SEQUENCES

We recognize an intermediate scale of depositional cyclicity not reported by Elrick and Read (1991). Five intermediate sequences (~15-30 m thick), are composed of stacked subtidal cycles and are defined by clear recessive to more resistant outcrop-weathering patterns typified by fine-grained, deep-water facies overlain by coarser grained, shallower water facies (Fig. 3A & Fig. 7). The majority of intermediate sequences contain 6 cycles, thus given the duration of cycles calculated by Elrick and Read (1991), intermediate sequences range from ~200-600 ky.

4.1.6.3 DEPOSITIONAL SEQUENCES

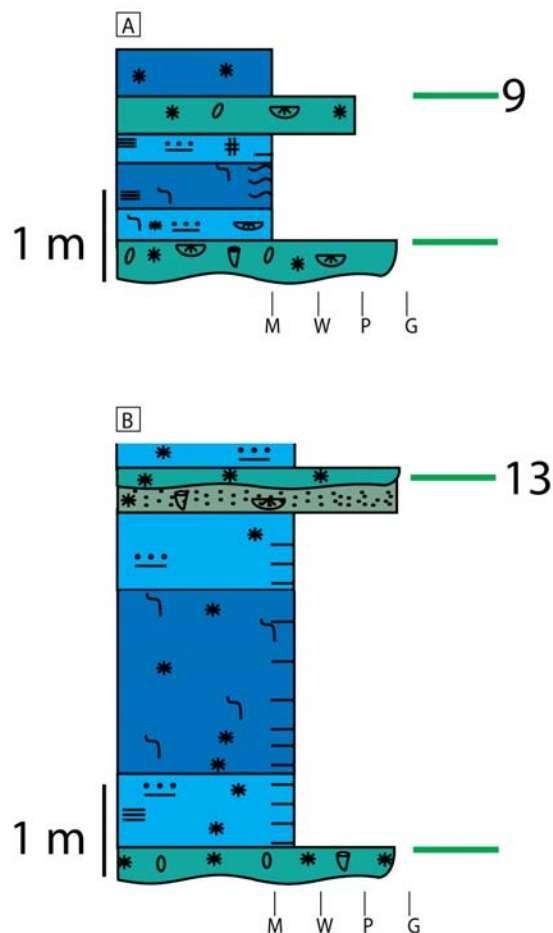
The single, full My-scale depositional sequence (~65 m thick) recognized in this study was identified from outcrop-weathering patterns, facies distribution (cycle types), and cycle thicknesses with respect to systems tracts. It is equivalent to My-scale depositional Sequence 2 of Elrick and Read (1991). There are relatively weak systematic cycle-stacking and cycle-thickness patterns associated with My-scale depositional sequences. When accommodation is low



Explanation				

Figure 7: Stratigraphic column of targeted Woodhurst member. Systems tracts of My-scale depositional sequence highlighted in orange, blue, green, and black arrows. Systematic cycle stacking and thickness patterns are not observed for intermediate sequences (light-blue boundaries). SPL (Sacagawea Peak Lower) represents the basal 14.4 m of the measured section. The upper SPL section directly underlies the SP (Sacagawea Peak) section ~75 m thick. [Note PSC cycles are located throughout stratigraphic section, while SC cycles are most abundant in LSTs and HSTs]

Transgressive-Regressive



Regressive

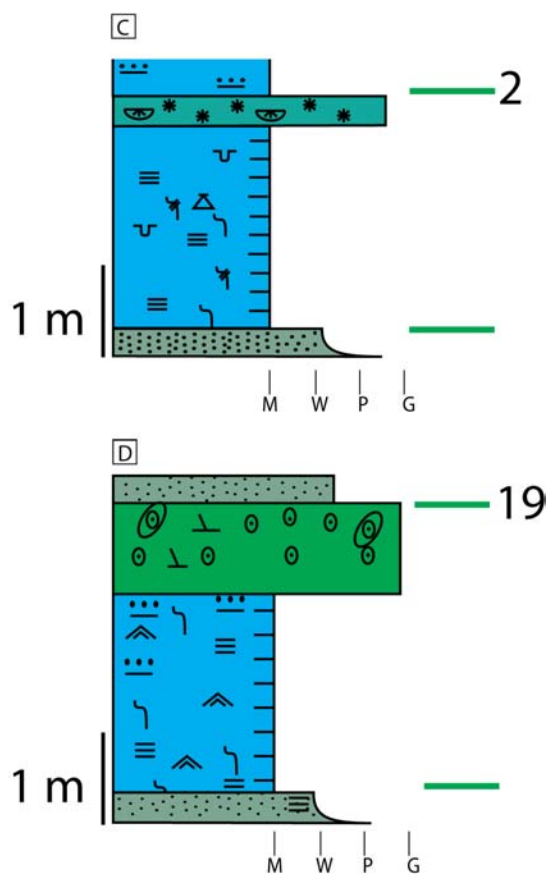


Figure 8: Examples of Woodhurst transgressive- and transgressive-regressive cycles displaying PSC and SC facies stacking patterns. **(A)** Cycle 9, a transgressive-regressive PSC cycle. **(B)** Cycle 13, a transgressive-regressive SC cycle. **(C)** Cycle 2, regressive PSC cycle **(D)** Cycle 19, a regressive SC cycle.

(LST and late HST) cycles are thinner than average and SC cycles are present. Cycles within LSTs of depositional sequences 2 and 3 have average cycle thicknesses of 2.0 and 4.0 m, respectively. Whereas, cycles located in the TST and early HST of My-scale depositional Sequence 2 show an average thickness of 7 m, and are typically composed of PSC cycles.

4.2 LABORATORY RESULTS

4.2.1 WHOLE ROCK $\delta^{13}\text{C}_{\text{carb}}$ VALUES

Whole rock $\delta^{13}\text{C}_{\text{carb}}$ values range from 4.3 ‰ to 7.5 ‰ (average = 5.0 ‰) (Appendix 2). These relatively high $\delta^{13}\text{C}_{\text{carb}}$ values are consistent with previously reported values from coeval deposits in the western U.S. (Nevada), the U.S. midcontinent (Iowa, Illinois, Indiana, Kansas, Missouri, Nebraska, Oklahoma, Texas), Russia, and Belgium (Mii et al., 1999; Saltzman et al., 2004), and display a previously reported major positive excursion peaking at 7.5 ‰ in the upper *S. isosticha* conodont Zone (Saltzman, 2002). $\delta^{13}\text{C}_{\text{carb}}$ values across the majority of cycles do not show systematic trends (see below), however, three cycles do exhibit a systematic cyclic trend, cycles 9, 16, and 18 (see below).

4.2.2 CONODONT SEM IMAGES

Conodonts from two samples (SPL 6.25 and SP 18.6) were imaged using the FEI Quanta 3D Dualbeam FEGSEM at the University of New Mexico in low-vacuum conditions with an electron beam accelerating voltage of 30kV and 140 pA current. These samples were chosen because they are representative of all

Woodhurst conodonts extracted at the study area. Elements exhibit CAI values of 3 or less, indicating thermal alteration of ~50-200 °C (Epstein et al., 1977; Fig. 9). Assuming a typical geothermal gradient (30 °C/km) the CAI temperature association corresponds to a burial-depth range of 1.5- 6.5 km. SEM images confirm findings of previous studies (e.g., Nöth, 1998; Blanco-Ferrara et al., 2011) that conodont elements with low CAI values (< 4) do not exhibit diagenetically altered textures (Fig. 10).

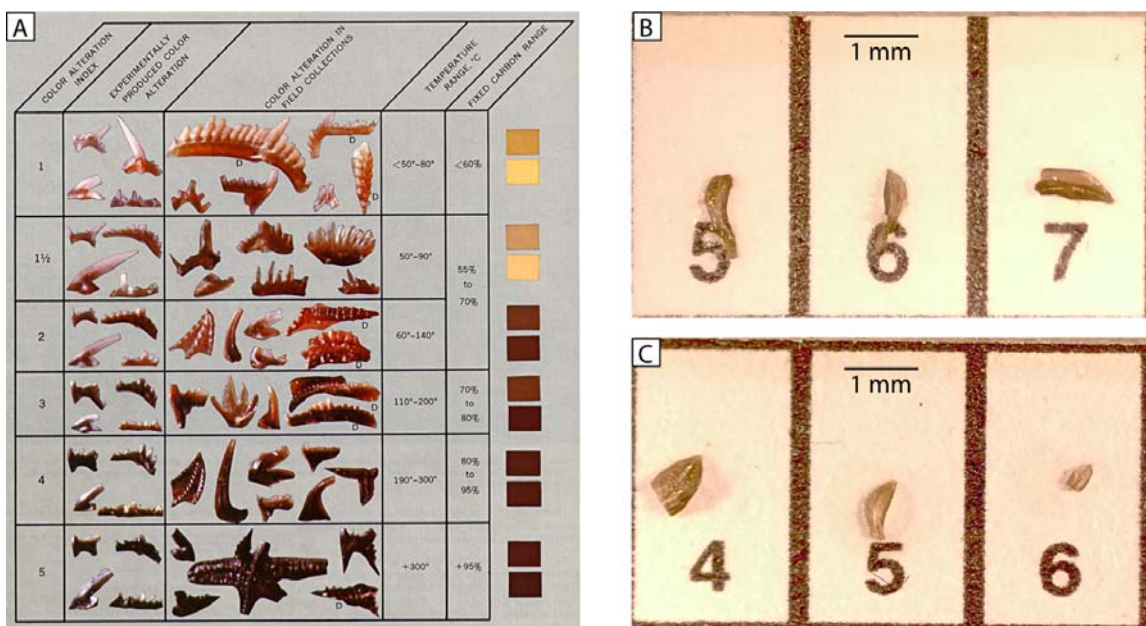


Figure 9: (A) Conodont alteration index (CAI) from Epstein (1977). (B) Typical platform elements. SPL 6.25 (5&6) *Siphonodella obsoleta* (7) *Polygnathus inornatus*. (C) Conodont platform elements from SP 18.6 (4&6) *Siphonodella obsoleta* (6) *Polygnathus communis*; Gilbert Klapper, University of Iowa (personal comm., 2009) CAI < 3 (representing thermal alteration of less than 200 °C)

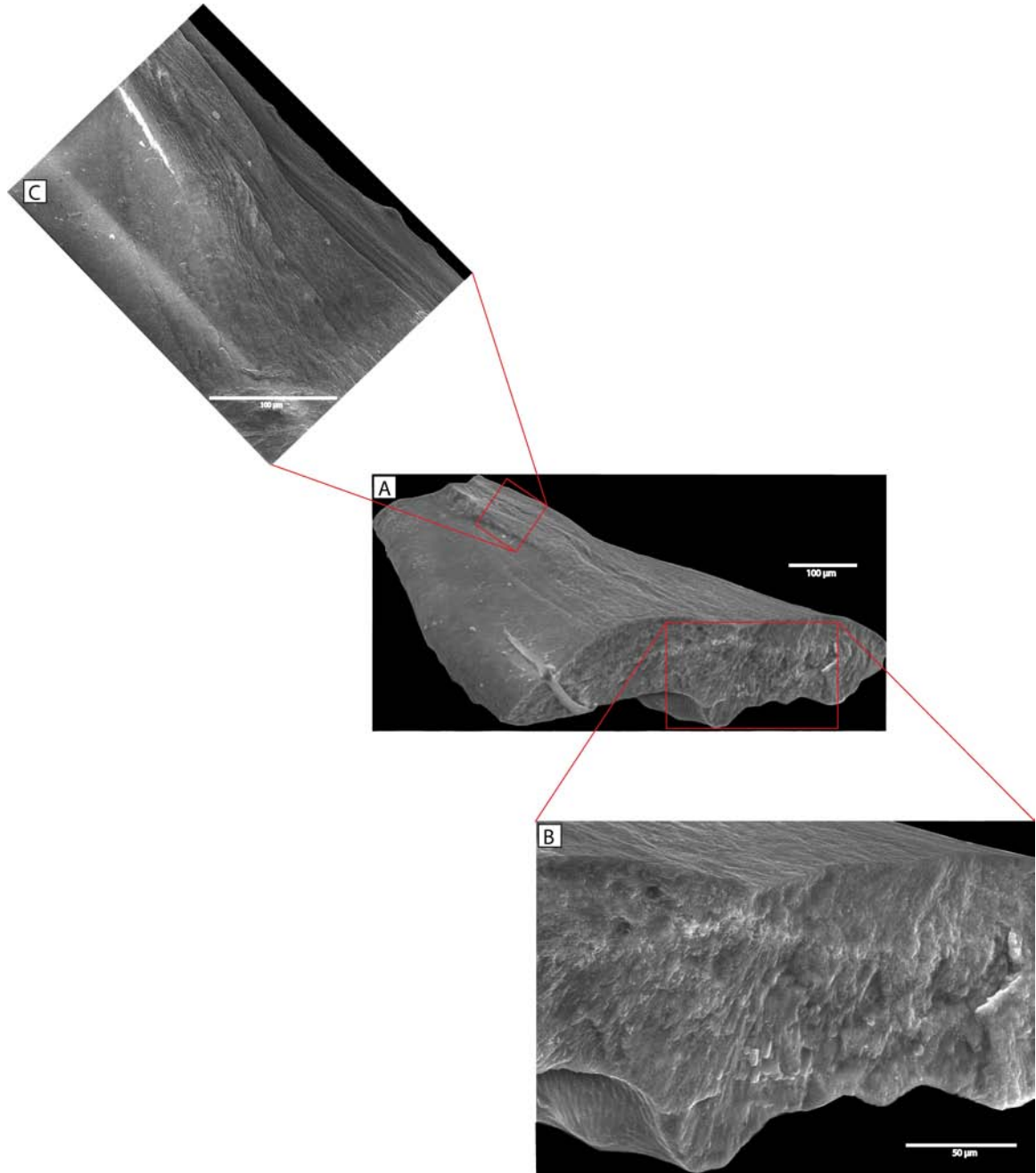


Figure 10: SEM images of a Woodhurst conodont element with CAI of < 3 (from SPL 6.25 *S. obsoleta*) **(A)** Posterior view of an incomplete *S. obsoleta* conodont element. **(B)** High resolution cross-section image (note pristine texture). **(C)** High resolution image of growth rings. **(B & C)** indicate original mineralogical textures. Image taken by C. Brunner.

4.2.3 $\delta^{18}\text{O}_{\text{apatite}}$ VALUES

Oxygen isotope values derived from conodont apatite ($\delta^{18}\text{O}_{\text{apatite}}$) range from 18.0 ‰ to 21.6 ‰ (average 19.4 ‰) (Fig. 11A). The $\delta^{18}\text{O}_{\text{apatite}}$ values (Appendix 3) are consistent with the ranges reported from coeval deposits in Spain and Ireland (Buggisch et al., 2008). The long-term $\delta^{18}\text{O}_{\text{apatite}}$ trend across the ~90 m measured section is cyclic, values are relatively high in the late HST of My-scale depositional sequence 1, decrease in the LST of My-scale depositional sequence 2, and begin to rise throughout the TST and get relatively high again in the late HST of My-scale depositional sequence 2. The observed long-term cyclic trend is consistent with the reports of Buggisch et al. (2008) (Fig. 11B).

$\delta^{18}\text{O}_{\text{apatite}}$ values recorded within five sampled cycles exhibit one distinct trend (Fig. 12BCD), a steady increase in $\delta^{18}\text{O}_{\text{apatite}}$ values across the cycle with the lowest values occurring in deep water facies near the cycle base and the highest values in the shallow facies or near the cycle cap. Values within cycle 9 (Fig. 12A) show a decrease in $\delta^{18}\text{O}_{\text{apatite}}$ values followed by an increase with the lowest values occurring in deep water facies; the latter portion of this trend is similar to the dominant trend, however, the values are all within uncertainty, so the trend is disregarded. Values within cycle 1 (Fig 12E) displays an opposite pattern to the dominant trend; with higher values occurring in deep-water facies near the cycle base and the lowest values in the shallow facies or near cycle cap. This cycle only contains two data points, and we are not confident in calling this a

trend, so we disregard the values. The magnitudes of isotopic shift across cycles exhibiting the dominant trend range from 0.7-2.5 ‰ (mean 1.4 ‰).

5. DISCUSSION

5.1 STRATIGRAPHIC CYCLICITY

5.1.1 DEPOSITIONAL SEQUENCE

Observed systematic cycle-stacking and cycle-thickness patterns within the Woodhurst My-scale depositional sequence represent a combination of typical characteristics reported in both greenhouse and icehouse sequences. Greenhouse sequences display long-term retrogradation and progradation of facies (Lehrmann and Goldhammer, 1999). Cycles within the progradational portion of a greenhouse sequence (LST late HST) typically thin upward while shallow-water facies (e.g., peritidal facies) become more prominent, whereas cycles within retrogradational units (TST and early HST) thicken upward and are composed of open marine facies (Lehrmann and Goldhammer, 1999). Cycles within icehouse sequences often display evidence of high-amplitude sea-level fluctuations i.e., subaerial exposure, and exhibit nonsystematic facies-stacking and cycle-thickness patterns (Lehrmann and Goldhammer, 1999; Elrick and Scott 2010). Cycles within the Woodhurst sequence were not subaerially exposed, but facies juxtapositions indicate large-amplitudes of sea-level fluctuation. SC cycles become more abundant during zones of low accommodation (late HST Sequence 1, LST Sequence 2), but they are still not

the dominant cycle type. These characteristics are descriptive of icehouse conditions. However, varying cycle thickness within zones of low and high accommodation, along with the dominance of the shallowest water facies in the LST of Sequence 3 suggest greenhouse conditions.

5.1.2 INTERMEDIATE SEQUENCES

Sea-level amplitudes associated with intermediate sequences were probably subdued because distinct systems tracts other than MFZs are not obvious. There is no systematic relationship between cycle types and clearly defined recessive-resistant intervals observed in the outcrop-weathering pattern. The reasons for this are unclear; perhaps the percentage of marl within both rhythmite facies is greater at the base of intermediate sequences allowing for more physical weathering, or potentially subtle grain-size differences exist between deep-water facies at the base and top of intermediate sequences. They also display a lack of systematic thicker-than-average cycles deposited during the TST/MFZ followed by thinner-than-average cycles during the HST/LST (e.g., Lehrmann and Goldhammer, 1999). This is due to the fact that the Woodhurst Member in the study area accumulated along the deep ramp, and cycle thicknesses were not accommodation limited (Elrick and Read, 1991).

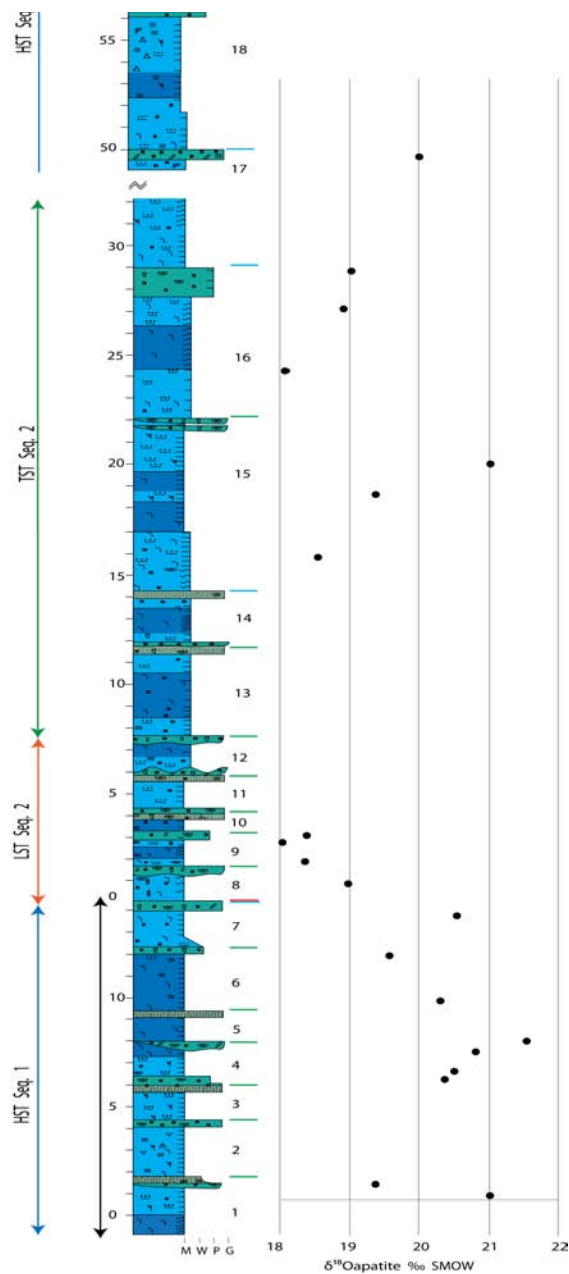


Figure 11 A: Long-term oxygen isotope trends across a condensed measured Woodhurst section at the study area. $\delta^{18}\text{O}$ values are cyclic; values are relatively high in the late HST of sequence 1, decrease in the LST of sequence 2, increase across the TST of sequence 2 into the HST of sequence 2. This cyclic pattern is similar to the long-term trends reported by Buggisch et al. (2008). Black line indicates SPL section (basal 14.2 m)

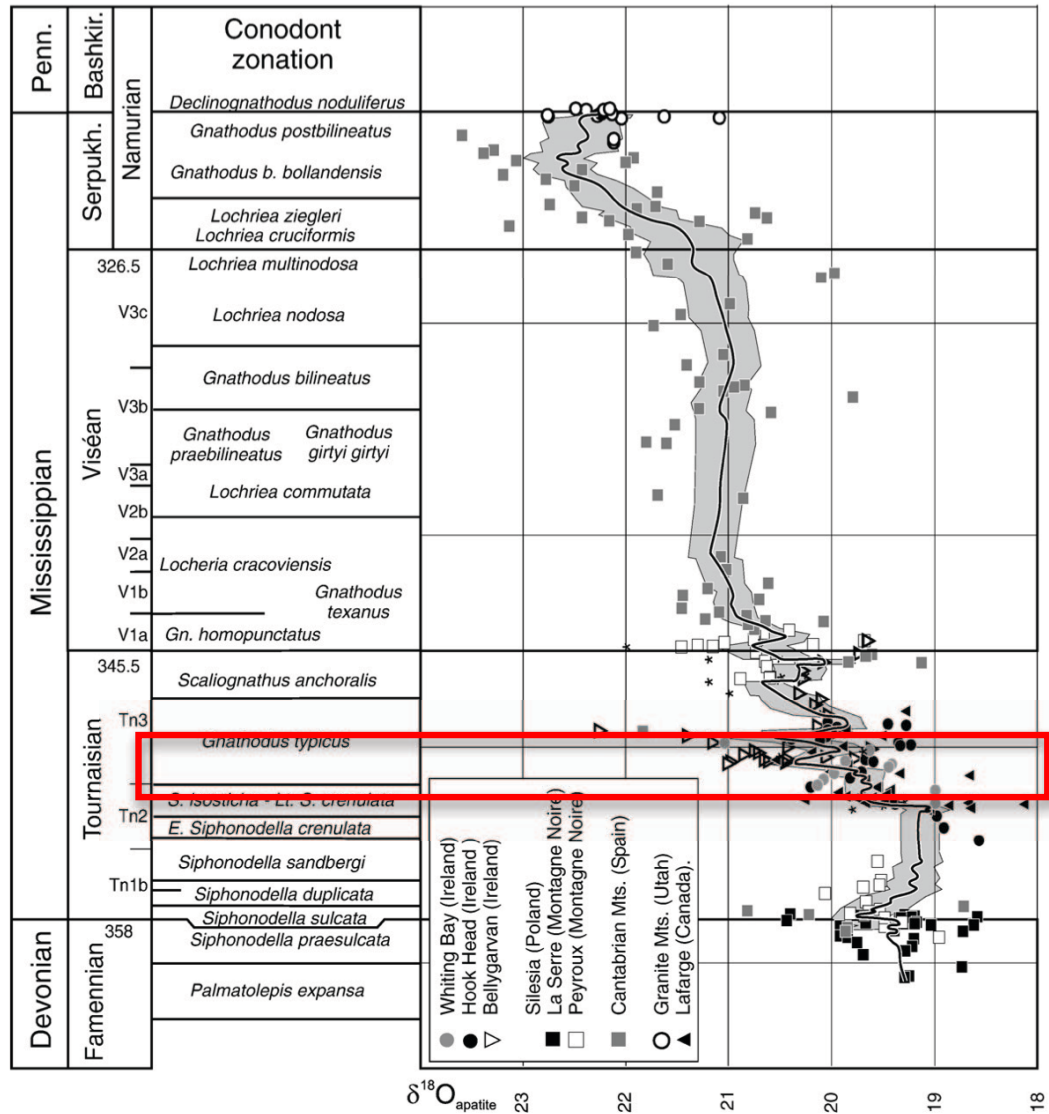


Figure 11 B: Long-term $\delta^{18}\text{O}$ values derived conodont apatite from Buggisch et al. (2008). The red box highlights the cyclic pattern of a coeval interval to long-term trend observed in southwest Montana.

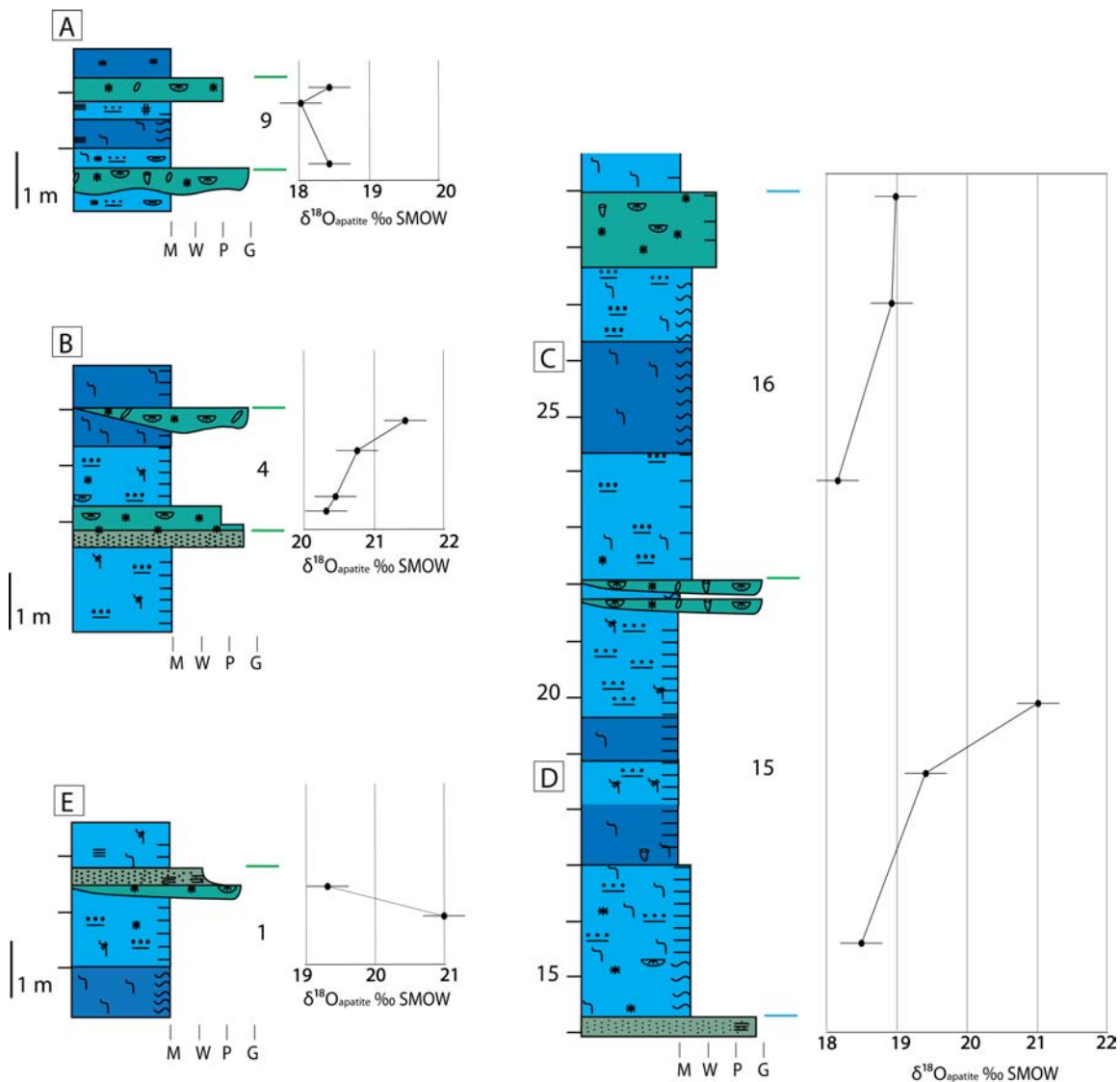


Figure 12: $\delta^{18}\text{O}_{\text{apatite}}$ values across five targeted high-frequency cycles. **(A)** $\delta^{18}\text{O}_{\text{apatite}}$ values across cycle 9 decrease then increase with the lowest $\delta^{18}\text{O}_{\text{apatite}}$ values occurring in deep water facies. Values are all within error, so the trend is disregarded. **(B) (C) (D)** Cycles 4, 16, and 15 respectively, displaying the dominant trend, $\delta^{18}\text{O}_{\text{apatite}}$ values increase steadily across cycles with lowest values in deep water facies near the cycle base and highest values in shallow water facies (cap) or near the cycle cap. **(E)** Cycle 1 showing an opposite pattern, higher $\delta^{18}\text{O}_{\text{apatite}}$ values in deep water facies and low $\delta^{18}\text{O}_{\text{apatite}}$ values in shallow water facies. Horizontal colored lines are equivalent to figure 7.

5.1.3 HIGH-FREQUENCY CYCLES

Approximately half of the observed Woodhurst cycles record transgressive-regressive facies stacking patterns. Such facies stacking patterns are expected given a typical sea-level rise and fall succession; however, many cyclic successions in the geologic record display only regressive stacking patterns (e.g., Markello and Read, 1982; Calvet and Tucker 1988; Oslegar, 1991; Oslegar and Read, 1991; Goldhammer et al., 1993). These regressive or upward-shallowing patterns have been explained by 1) a rapid onset of sea-level rise preventing deposition of transgressive facies, 2) a ravinement (or erosional) surface, which erodes previously deposited transgressive facies resulting in deposition of deeper-water facies directly over the underlying cycle cap. We suggest these scenarios for regressive PSC cycles and for regressive SC cycles respectively.

SC cycles (substorm wave base deposits directly overlain by upper shore face facies) provide the strongest evidence for significant magnitudes of sea-level rise and fall because the facies accumulated from water depths spanning several 10's of meters.

5.2 CYCLE $\delta^{18}\text{O}_{\text{apatite}}$ TRENDS

An observed $\delta^{18}\text{O}_{\text{apatite}}$ trend (cycles 4, 15, and 16) supports the hypothesis that the Woodhurst high-frequency cycles were driven by glacial eustasy in combination with changes in surface seawater temperatures (SST) (Fig. 12). Decreasing and low $\delta^{18}\text{O}_{\text{apatite}}$ values occur within deep-water facies

deposited during sea-level rise and highstand (interglacial period), while increasing and high values occur in shallow water facies deposited during sea-level fall and lowstand (glacial periods). In addition to changes in ice volume, the documented isotopic trends are also supported by high-frequency SST changes. When seawater temperatures decrease (i.e., glacials) the fractionation between minerals and seawater increases resulting in higher $\delta^{18}\text{O}$ values in marine minerals in equilibrium with seawater. Conversely, with warmer SSTs (interglacial) the opposite trend is observed, i.e., lower $\delta^{18}\text{O}$ values in marine minerals in equilibrium with seawater (Fig. 13).

Theoretically, $\delta^{18}\text{O}$ trends should mirror the relative sea-level curve. Conceivably, the trend observed in cycles, 4, 15, and 16 (Fig. 12B,C,D) could represent the upper (regressive) portion of the expected trend. Had cycles 4, 15, and 16 been sampled at a finer resolution near the cycle base, then those values may record higher $\delta^{18}\text{O}_{\text{apatite}}$ values, resulting in a trend similar to that of the expected.

Magnitudes of isotopic shift across Lower Mississippian cycles range from 0.7-2.5 ‰ (mean 1.4 ‰), and are similar to magnitudes of shifts across Pleistocene glacial-interglacial cycles, typically varying around 1-2 ‰ (Mix et al., 1995; Lisicki and Raymo, 2005; Ruddiman, 2008). Pleistocene $\delta^{18}\text{O}$ trends are typically symmetrical in shape, while the dominant trend observed in Lower Mississippian cycles are asymmetrical. This asymmetric shape is due to a relatively coarse sampling resolution.

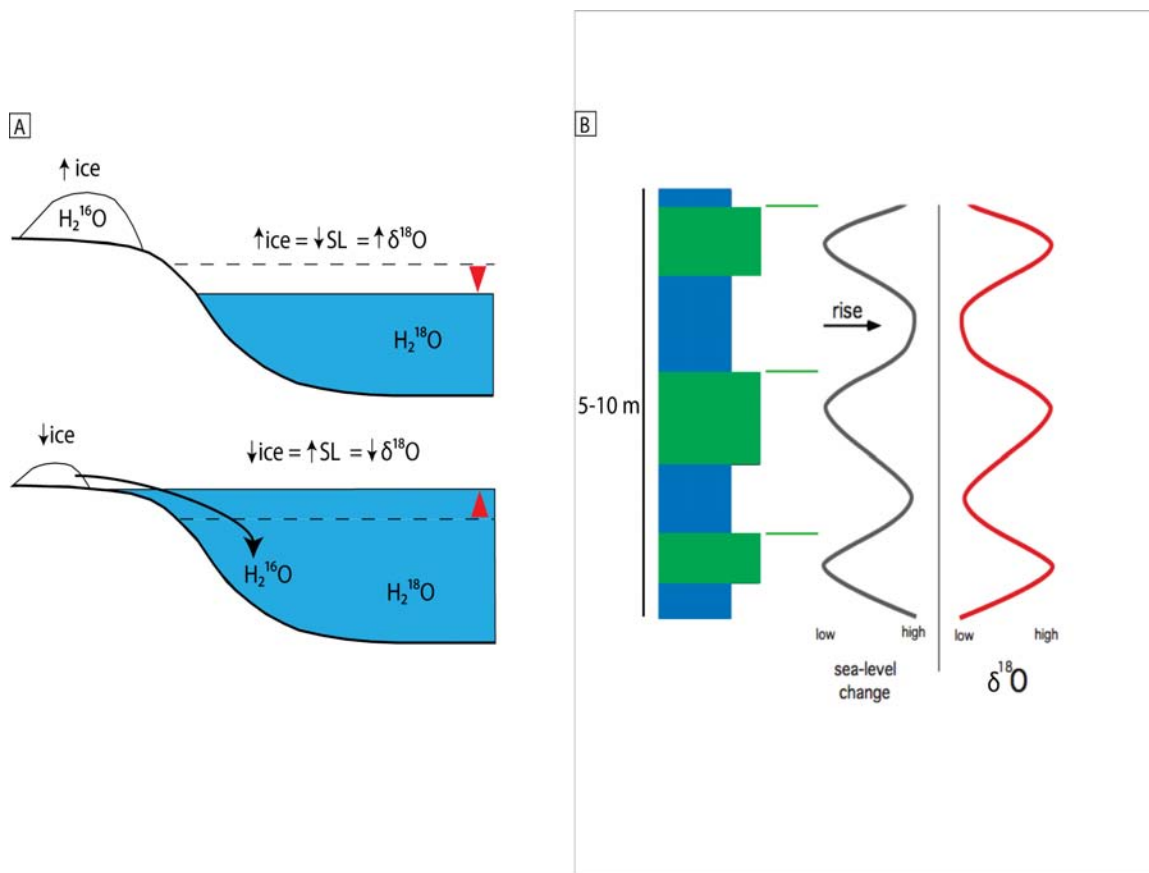


Figure 13: Relationships between $\delta^{18}\text{O}_{\text{apatite}}$ trends, ice volume, and glacio-eustasy. **(A)** During glacial intervals, sea level is low and isotopically light water is locked in continental ice sheets, leaving the ocean enriched in isotopically heavy water. During interglacials, ice melts, sea level rises, and the $\delta^{18}\text{O}$ value of the ocean decreases due to enrichment of isotopically light water. **(B)** Relationship between stacked cycles and the expected $\delta^{18}\text{O}$ relationship if cycles were generated by glacio-eustasy. Blue boxes indicate deep-water facies, green boxes indicate shallow water facies, and horizontal-green lines represent cycle boundaries. [Note $\delta^{18}\text{O}$ trends and relative sea-level change are mirror images]

5.3 PALEOCLIMATE INTERPRETATIONS

$\delta^{18}\text{O}$ values are a proxy for combined effects of salinity (evaporation), temperature and ice-volume changes. This study will be focusing on interpreting temperature and ice-volume effects because fossil assemblages indicate normal marine salinities. In post-Cretaceous paleoclimate studies, independent proxies (e.g., TEX-86 or alkenone paleothermometry) can be used to determine the effects of temperature leaving the remaining $\delta^{18}\text{O}$ values a result of the ice-volume effect. Unfortunately, such tools cannot be applied to pre-Cretaceous deposits, therefore, it is not straightforward estimating the affects of SST versus ice-volume changes for this study.

Estimated Early Mississippian tropical SSTs from conodont apatite were calculated using the equation reported by Kolodny et al. (1983).

$$T[^\circ\text{C}] = 113.3 - 4.38(\delta^{18}\text{O}_{\text{apatite}} - \delta^{18}\text{O}_{\text{water}}) \quad (1)$$

Assuming a $\delta^{18}\text{O}_{\text{sea}}$ value of 0.0‰, the reported 18.0 to 21.6 ‰ range of $\delta^{18}\text{O}_{\text{apatite}}$ values from this study, correspond to SST's ranging from ~ 34 to 19 °C, respectively. However, recently Pucéat et al. (2010) presented a revised phosphate–water oxygen isotope fractionation equation based on oxygen isotopes determined on fish apatite raised in aquariums at controlled temperatures with monitored water oxygen isotope compositions.

$$T[^\circ\text{C}] = 118.7(\pm 4.9) - 4.22(\pm 0.20)(\delta^{18}\text{O}_{\text{apatite}} - \delta^{18}\text{O}_{\text{water}}) \quad (2)$$

The revised equation is similar to *equation (1)* but has major implications for previously calculated paleoclimatic reconstructions derived from oxygen isotopes of biogenic apatite; if this equation is correct then calculated paleotemperatures have been underestimated by 4-8 °C when using the Kolodny equation. Using the Pucéat et al. (2010) equation (also assuming a $\delta^{18}O_{water}$ value of 0.0 ‰) the Early Mississippian $\delta^{18}O_{apatite}$ values result in SST's ranging from ~27-42 °C, respectively, showing a calculated difference of 8 °C from the Kolodny to Pucéat equation. When comparing Early Mississippian SSTs to tropical-subtropical Last Glacial Maximum (LGM) paleotemperatures, calculated from Sr/Ca ratios, Beck et al. (1997) report SSTs ranging from 18-23 °C, and comparing modern (interglacial) tropical SSTs (23-28 °C), it is clear that Early Mississippian SSTs associated with glacial-interglacial periods are much significantly higher.

If the $\delta^{18}O_{apatite}$ shifts (0.7 ‰-2.5 ‰; mean = 1.4 ‰) across individual Woodhurst cycles were strictly due to SST changes, then this would equate to a ~3-11°C glacial-interglacial SST change. During the LGM, tropical SSTs were ~5°C cooler (Beck et al. 1997; Ruddiman, 2002) than the Holocene. Using this as a guide, it is unlikely that the changes between Early Mississippian glacial-interglacial phases were larger than those reported for the Quaternary, particularly given previous warm paleoclimate interpretations for the Early Mississippian (Frakes et al., 1992); therefore, the upper end of the calculated temperature range likely represents too great of SST change.

Over the last century the estimated rise in sea level due to the ~ 0.5 °C increase in global mean SST is less than 5.0 cm (de Wolde et al., 1995). Extrapolating this to the estimated maximum $\sim 2\text{--}11$ °C SST for the Early Mississippian corresponds to thermal–eustatic changes of <1 m. The observed facies stacking patterns in Woodhurst cycles indicate significantly greater sea-level changes; i.e., the abrupt juxtaposition of substorm wave base through upper shoreface facies indicate sea-level fluctuations on the order of a few tens of meters, and argues against thermo-eustasy as the main driver for high-frequency cycle formation.

Conversely, if isotopic shifts across cycles were propelled by changes in ocean chemistry related to the ice-volume effect, then reported isotopic shifts (0.7-2.5 ‰) are equivalent to $\sim 60\text{--}250$ m sea-level changes, respectively (assuming 0.11‰/10 m; Fairbanks and Matthews, 1978). Magnitudes much greater than $\sim 50\text{--}75$ m (e.g. Heckel, 1994; Elrick and Scott 2010) would likely result in cycle caps showing evidence of subaerial exposure (e.g., pedogenic alteration, brecciation, karstification), the Woodhurst cycles do not exhibit; therefore, we suggest that the upper-end sea-level magnitude estimates are not reasonable. Paleoclimate interpretations due to only temperature changes or only ice-volume changes are unreasonable, so like the Quaternary, we suggest a combination of SST changes and glacial ice waxing and waning as the driver for oxygen isotopic shifts across Woodhurst cycles.

When interpreting pre-Cretaceous marine $\delta^{18}\text{O}$ shifts associated with glacial-interglacial cycles, a common question arises; how much of the shift is

due to changes in temperature versus ice volume? There currently is no way of partitioning the effects of ice versus temperature for Early Mississippian $\delta^{18}\text{O}_{\text{apatite}}$ shifts, however, they can be bracketed. Mix (1987) measured marine $\delta^{18}\text{O}$ values from planktonic and benthic forams from the LGM to Holocene and determined that at least 70% of the glacial-to-interglacial $\delta^{18}\text{O}$ shift results from the change in oceanic chemistry due to the ice effect, leaving the remaining 30% due to the temperature effect. In a similar study for the early Oligocene, Pekar et al. (2002) and Pekar and Chrisite-Blick (2003) determined that at least half of observed $\delta^{18}\text{O}$ shifts were due to temperature, while for the warm climates of the early Eocene Pekar et al. (2005) suggest that 70% of $\delta^{18}\text{O}$ shifts are the product of SST change, leaving the remaining 30% due to ice-volume effect. The varying influences of SST versus ice effect within $\delta^{18}\text{O}$ shifts are a function of the overall paleoclimate conditions, which control ice sheet size, $\delta^{18}\text{O}$ values of the ice, and the extent of Rayleigh Fractionation during warm and cool global climates.

These end-member relationships can be utilized to bracket the range of potential SST changes and glacio-eustatic sea-level magnitudes for the Early Mississippian (Table 2). Dividing isotopic shifts into appropriate percentages, ice effect can be calculated by the 0.11 ‰/10m relationship reported by Fairbanks and Matthews (1978), while temperature effect can be calculated by assuming 0.23 ‰/1°C. The mean isotopic shift across Woodhurst cycles is ~1.4 ‰; so applying the Quaternary ~70-30 % relationship to this mean shift corresponds to a ~1.0 ‰ shift due to the ice-volume effect and ~0.4 ‰ to the temperature effect. This ~1.0 ‰ shift equates to a glacio-eustatic sea-level change of ~ 90 m, while

the 0.4 ‰ shift is equivalent to a ~ 2 °C SST change. Applying the warm climate relationship of Pekar et al. (2005) to the mean 1.4 ‰ shift suggests a ~ 40 m glacio-eustatic sea-level change associated with a ~4.0 °C SST change.

While the Quaternary and Eocene examples provide an estimate for the potential range of combined sea-level magnitudes and SST changes, perhaps the climatic conditions during the Early Mississippian lay somewhere in between the cool Quaternary and warm Eocene, so we calculate values where the ice-volume

Cycle #	Isotopic shift (‰)	LGM		e. Eocene
		Ice: 70% Temp: 30%	Ice: 50% Temp: 50%	Ice: 30% Temp: 70%
16	0.7	45 m 1.0°C	30 m 1.5°C	20m 2.0°C
4	1.2	75 m 1.5°C	55 m 2.5°C	30 m 3.5°C
15	2.5	160 m 3.0°C	110 m 5.5°C	70 m 7.5°C
Mean	1.4	90 m 2°C	65 m 3°C	40 m 4°C

Table 2: Calculated sea-level and SST changes from Fairbanks and Matthews (1978) and Mix (1987) (LGM), Pekar et al. (2005) (e. Eocene), and an intermediate scenario. All presented values are approximate. Sea-level fluctuations were rounded to nearest 5 m, while SST change was rounded to nearest 0.5 °C.

and temperature effect are equal. Given this 50-50% scenario, this translates to a ~65 m sea-level and ~ 3.0 °C SST change. Regardless of which scenario is utilized, the mean isotopic shifts correspond to substantial glacio-eustatic sea-level magnitudes of at least several 10's of meters and SST changes of several degrees, implying substantial high-frequency climatic shifts during the Early Mississippian, and in particular, significant changes in glacial ice volumes.

5.4 $\delta^{13}C_{carb}$

Oppo et al. (1995) report a well-established systematic relationship, over the last two million years, between $\delta^{18}O$ and $\delta^{13}C$ values from benthic foraminiferal calcite across Pleistocene glacial-interglacial cycles; $\delta^{13}C$ values are low during glacial periods (high $\delta^{18}O$ values) and high during interglacial periods. The magnitude of these Pleistocene $\delta^{13}C$ shifts range from 0.5-1.0 ‰. In order to determine if similar systematic trends were present during the Early Mississippian, a high-resolution carbon isotope dataset was obtained across 11 Woodhurst cycles from whole rock carbonate carbon ($\delta^{13}C_{carb}$).

$\delta^{13}C$ values from marine carbonates reflect the isotopic value of the total dissolved carbon (TDC) within the deep or shallow ocean, depending on where the mineral is being precipitated. On a short timescale (< 10 ky) the TDC is affected by influxes from mantle CO_2 degassing and continental weathering. Long-term (10^5 - 10^7 yr) changes in the TDC are a function of the burial ratio of inorganic (^{13}C) vs. organic (^{12}C) carbon, more often than not associated with the biological pump. The biological pump is a steady-state nonequilibrium fractionation between the TDC in the shallow and deep ocean due to high

biological activity in the shallow photic zone. Photosynthetic organisms preferentially incorporate ^{12}C into their tissue leaving the TDC of the shallow ocean enriched in ^{13}C , upon their death, their remains sink into the deep ocean, causing the TDC of the deep ocean to become enriched in ^{12}C (Sharp, 2007). During periods of increased productivity, a greater contrast develops between the TDC of the deep and shallow ocean.

Unlike oxygen isotopes, carbon isotopes are not affected by ice volume or temperature changes; however, Oppo et al. (1995) report a systematic relationship between $\delta^{18}\text{O}$ and $\delta^{13}\text{C}$ values and attributes this relationship to intensified atmospheric and ocean current dynamics, which bring an upsurge of nutrients to the surface ocean increasing the primary productivity of the surface ocean, therefore creating a greater contrast in the TDC between the deep and shallow ocean. Applying this scenario to Lower Mississippian cycles, one would expect to observe relatively high $\delta^{13}\text{C}_{\text{carb}}$ values during glacial periods (cycle caps), which are sourced from the shallow-surface water (skeletal material).

The long-term $\delta^{13}\text{C}_{\text{carb}}$ trend across the ~90 m sampled Woodhurst interval spans the upper *S. isosticha* and *G. typicus* conodont zones, and does not display a systematic trend within a My-scale depositional sequence framework. While the composite curve does not span the entire Woodhurst, the trend confirms a major global positive $\delta^{13}\text{C}_{\text{carb}}$ excursion peaking at ~7.5 ‰ in the upper *S. isosticha* conodont Zone (Fig. 14) (Saltzman, 2002; Saltzman et al., 2004). Saltzman et al. (2004) attribute the positive $\delta^{13}\text{C}_{\text{carb}}$ excursion to enhanced phosphate regeneration and biological pumping of ^{12}C into the

semirestricted, anoxic Antler foreland basin, which contains abundant evidence in the form of laminated organic-rich units (Saltzman et al., 2000).

This globally reported major positive carbon-isotope excursion is thought to have had major implications for the initial onset of the major LPIA glaciation. The increase in biological pumping of ^{12}C to the deep ocean from the surface ocean involves the sequestration of atmospheric CO_2 via photosynthesis. The drawdown of atmospheric CO_2 creates a positive feedback loop, allowing for less greenhouse-gas warming, consequently cooling the planet, and allowing for initial accumulation of ice sheets. Buggisch et al. (2008) report long-term $\delta^{18}\text{O}_{\text{apatite}}$ and $\delta^{13}\text{C}_{\text{carb}}$ trends across the Mississippian. The increase in $\delta^{18}\text{O}_{\text{apatite}}$ values from ~ 19.0 to ~ 21.0 ‰ is thought to represent initial climatic cooling and ice buildup of the LPIA (Fig. 15)

A closer examination of the globally reported positive carbon excursion reveals that the initial carbon excursion precedes the initial increase in $\delta^{18}\text{O}_{\text{apatite}}$ values. Buggisch et al. (2008) suggest this represents the initiation of CO_2 drawdown allowing for a cooling of the global Early Mississippian paleoclimate.

There are no reports of systematic $\delta^{13}\text{C}$ trends associated with interpreted glacial-interglacial cycles for deep-time studies. Unlike Pleistocene studies, which conduct $\delta^{13}\text{C}$ analyses on separate benthic and planktonic forams, Woodhurst $\delta^{13}\text{C}_{\text{carb}}$ values were taken from whole-rock samples and the majority of values display nonsystematic trends with respect to cyclostratigraphy. However, cycles 9, 16, and 18 display some ordered $\delta^{13}\text{C}_{\text{carb}}$ trends (Fig. 16).

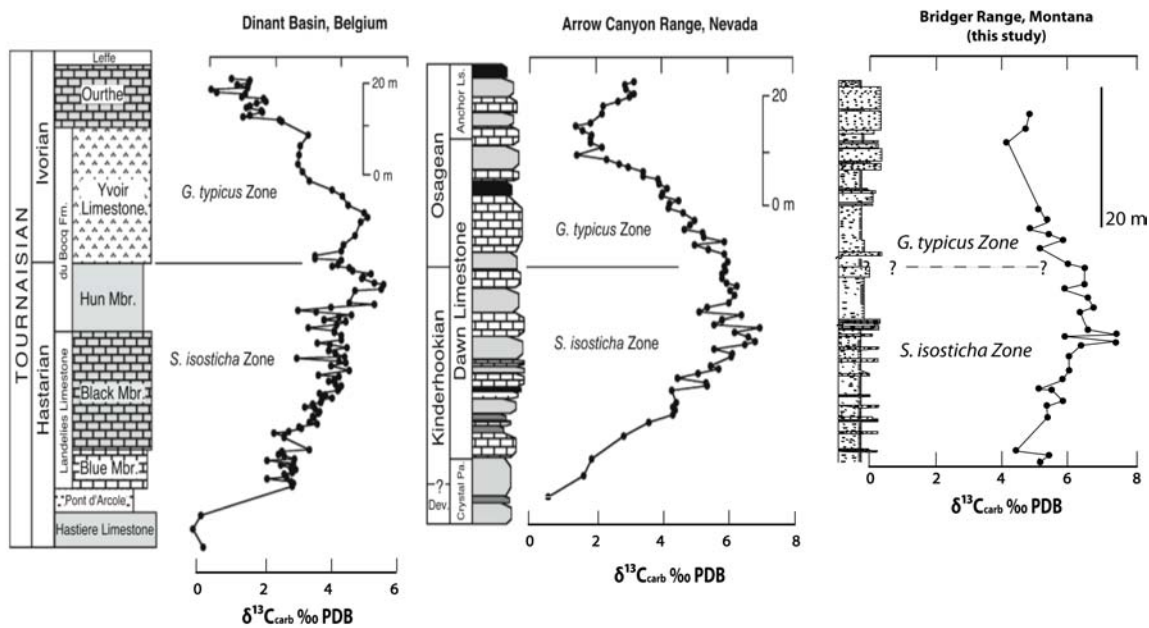


Figure 14: Globally recorded $\delta^{13}\text{C}_{\text{carb}}$ values from Saltzman et al. (2004) and this study. Lodgepole $\delta^{13}\text{C}_{\text{carb}}$ values confirm global trends of a major positive excursion peaking at $\sim 7.5 \text{‰}$ in the upper *S. isosticha* conodont Zone.

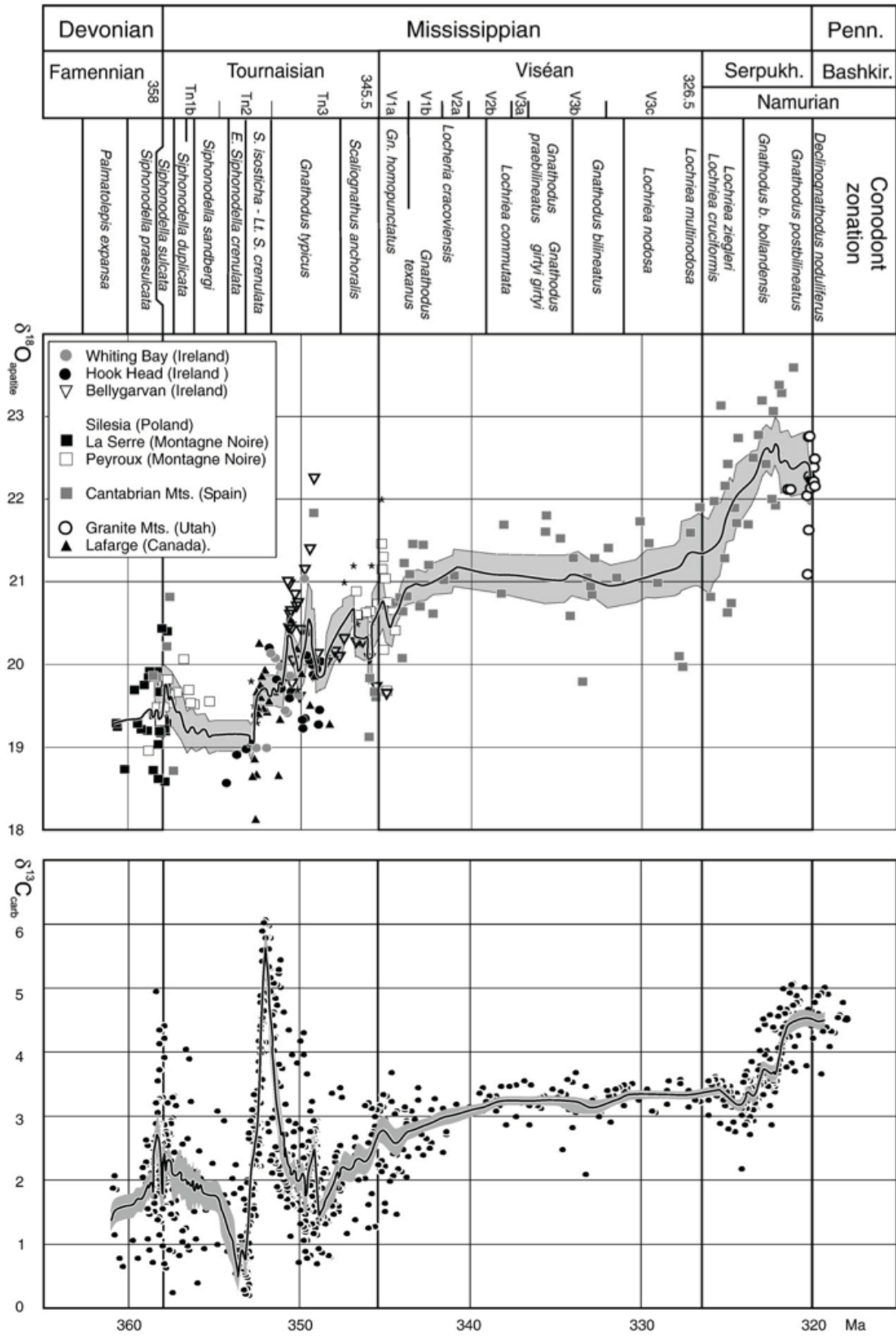


Figure 15: long-term carbon and oxygen isotope trends across the Mississippian from Buggisch et al. (2008). Note how the initial $\delta^{13}\text{C}_{\text{carb}}$ excursion precedes the initial increase trend in $\delta^{18}\text{O}_{\text{apatite}}$ values, which is thought to be due to increased atmospheric carbon dioxide drawdown allowing for the initiation of Gondwanan ice sheets.

These three cycles display deepening followed by shallow facies trends (transgressive-regressive cycles), which are mirrored by initially decreasing $\delta^{13}\text{C}$ values, and lowest values in the deepest water facies, followed by increasing values in the shallow facies. The magnitude of shift is ~ 1.0 ‰. These trends support the hypothesis of Oppo et al. (1995) that trends were due to an increase in primary productivity during glacial periods as suggested by Ruddiman (2002).

We suggest the lack of systematic trends observed across the majority of Woodhurst cycles is due to the mixture of deep and shallow water carbonate material which may record TDC values from a range of water depths and unknown vital effects.

5.5 IMPLICATIONS

The observed $\delta^{18}\text{O}_{\text{apatite}}$ trend across cycles suggests glacial-eustatic origins indicating the presence of continental ice waxing and waning on an orbital timescale. This implies that the LPIA initiated at least as early as the Tournaisian; approximately 25 My earlier than previously proposed (Hambrey and Harland, 1981; Crowell, 1983; Horbury, 1989; Frakes et al., 1992; Smith and Read, 1999, 2000; Gonzalez 2001; Wright and Vandstone, 2001; Fielding et al., 2008; Bishop et al., 2009, 2010). Other researchers (Caputo and Crowell, 1985;

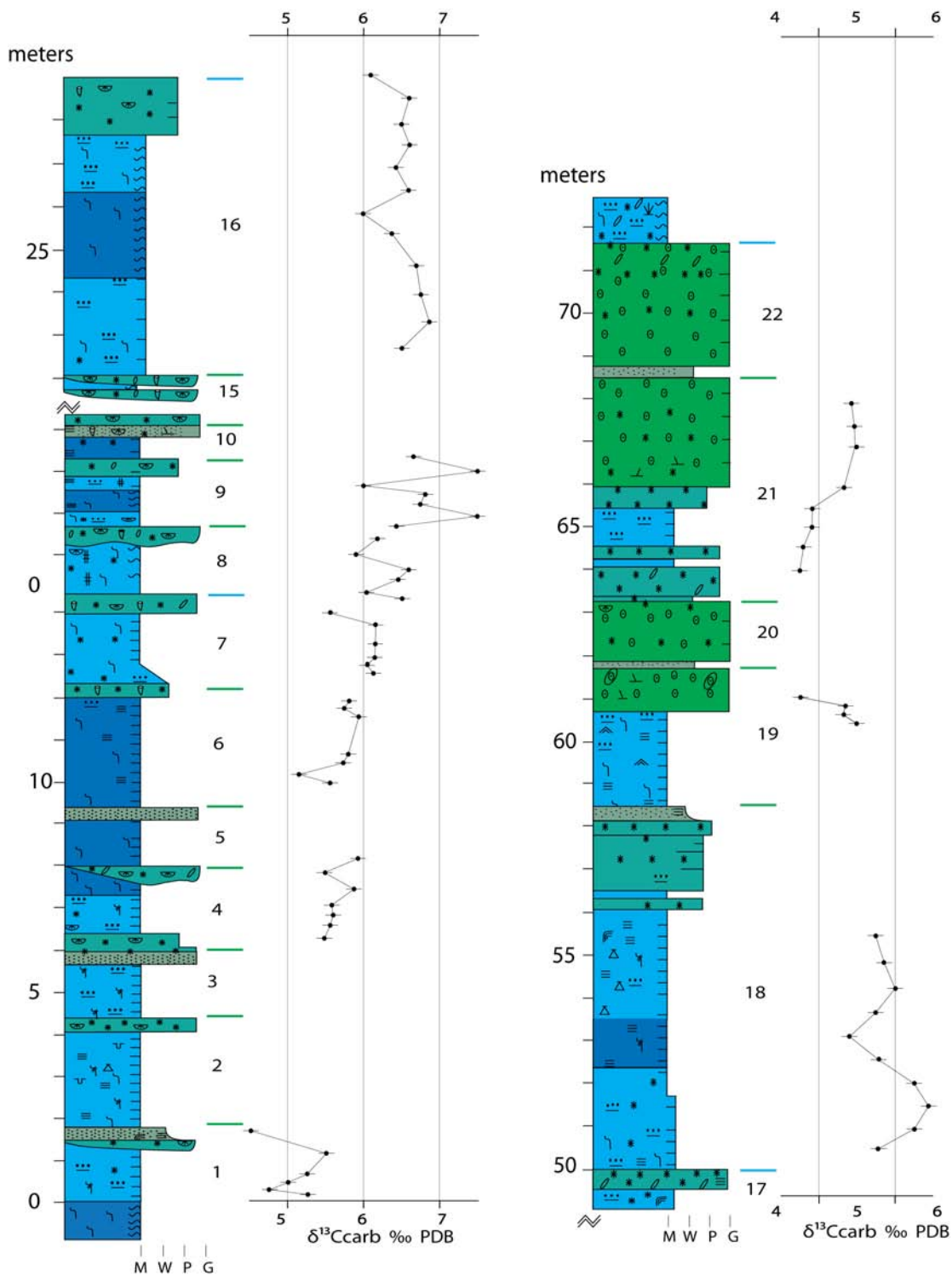


Figure 16: Condensed measured stratigraphic section displaying relationships between cycles and whole rock carbon isotope data ($\delta^{13}\text{C}_{\text{carb}}$). Note the lack of systematic $\delta^{13}\text{C}_{\text{carb}}$ trends across cycles. Horizontal colored lines same as Figure 7 and first 14 m represent SPL section.

Veevers and Powell, 1987; Buggisch et al., 2008) suggest the LPIA may have initiated in the Late Devonian through evidence of South American glacial deposits (Amazon Basin, Bolivia), reported global sea-level regression, and a minor positive $\delta^{18}\text{O}_{\text{apatite}}$ excursion in the latest Famennian through the Devonian-Carboniferous (D-C)

boundary. This evidence, combined with data presented in this study, and along with the overwhelming evidence reported by the Late Mississippian camp suggests the presence (or build up) of an ice sheet spanning the Late Devonian through Late Mississippian; a statement originally put forth by Veevers and Powell (1987).

Frakes et al. (1992) define the Devonian and Early Mississippian, globally, as a warm period based on reports of high-latitude distribution of carbonate and evaporite facies along with minimal evidence of glaciation. These warm indicators exist despite the evidence for ice implying that during this time interval, the planet was not uniformly warm but rather warm in some locations, and cool enough in others (high latitudes) for ice to form, wax, and wane on orbital timescales. This rock and isotopic based evidence for *concurrent* warm and cool conditions necessitates we broaden our traditional view of end member ice versus greenhouse paleoclimate conditions, and realize that warmer-greenhouse intervals can have short-lived cool intervals and cool-icehouse times can have brief warm episodes.

To put the Early Mississippian in perspective, sea-level fluctuations derived from the mean-isotopic shift (1.4 ‰) across Woodhurst cycles range ~

40-90 m. These magnitudes are much less than those reported for known cool-icehouse conditions of the Pennsylvanian and Pleistocene (> 100 m) (e.g., Fairbanks, 1989; Heckel, 1994; Chappell et al., 1996; Cutler et al., 2003; Joachimski et al., 2006), however, they are greater than reported warm-greenhouse conditions (~ 20-40 m) (Osleger, 1991; Goldhammer et al., 1993; Pekar et al., 2005). These estimated sea-level magnitudes suggest the Early Mississippian is more representative of a transitional paleoclimate.

If the present day East-Antarctic ice sheet (EAIS) melted researchers suggest a corresponding sea-level rise of ~ 60 m (Pekar et al., 2005); therefore, if our interpretation of Tournaisian sea-level fluctuations calculated from the mean isotopic shift are correct, then this equates to an ice sheet ranging from 0.5-1.25 times the size of the present day EAIS during the Early Mississippian.

6. CONCLUSIONS











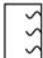















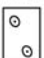


- 1) The Woodhurst member of the Lodgepole Formation in the Bridger Range of southwest Montana is composed of five facies types, representing deposition from offshore regions to upper shoreface interior ramp environments (along a distally steepened carbonate ramp).
- 2) Facies exhibit regressive- and transgressive-regressive stacking patterns forming subtidal cycles (22 cycles 1-8 m thick) capped by either proximal storm or shoal deposits. Cycles stack into 5 intermediate sequences

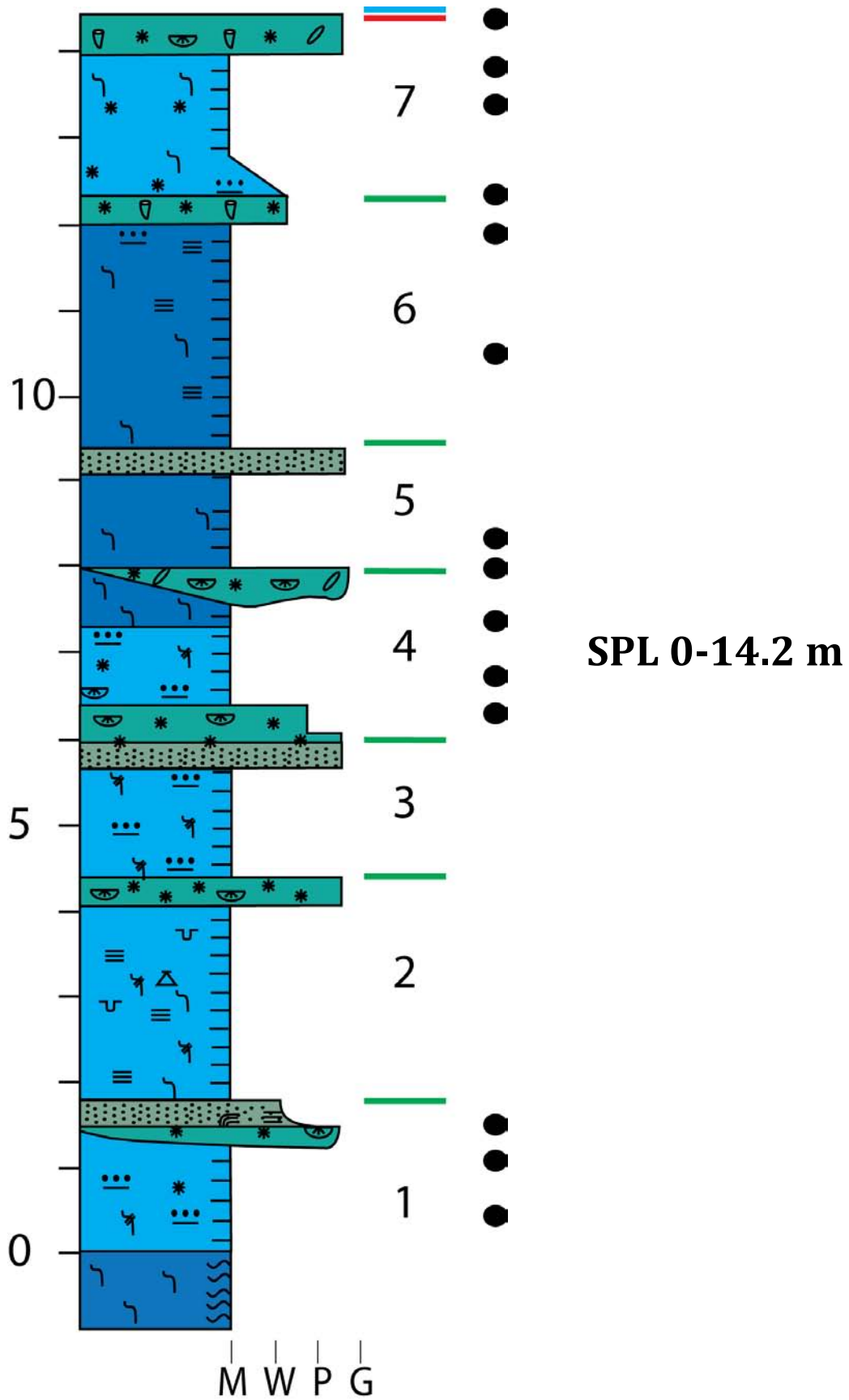
(~15-30 m thick); 4 of which group into a single full My-scale depositional sequence.

- 3) Facies stacking patterns suggest similar magnitudes of sea-level fluctuations across cycles and intermediate sequences.
- 4) Carbon-isotope trends across 11 individual subtidal cycles do not display systematic trends related to cycle formation, but the long-term composite curve confirms previously reported global trends (Saltzman) of a significant positive excursion, peaking at ~ 7.5 ‰, in the upper *S. isosticha* conodont Zone.
- 5) Oxygen-isotope trends across 4 targeted cycles support glacio-eustatic origins along with SST changes; sea-level fluctuations ranging from 30-75 meters imply that the possibility of an EAIS-size ice sheet waxing and waning during the Early Mississippian. If correct, ice this size implies the LPIA started at least 25 my earlier than previously suggested (Hambrey and Harland, 1981; Crowell, 1983; Horbury, 1989; Frakes et al., 1992; Smith and Read, 1999, 2000; Gonzalez 2001; Wright and Vandstone, 2001; Fielding et al., 2008; Bishop et al., 2009, 2010).

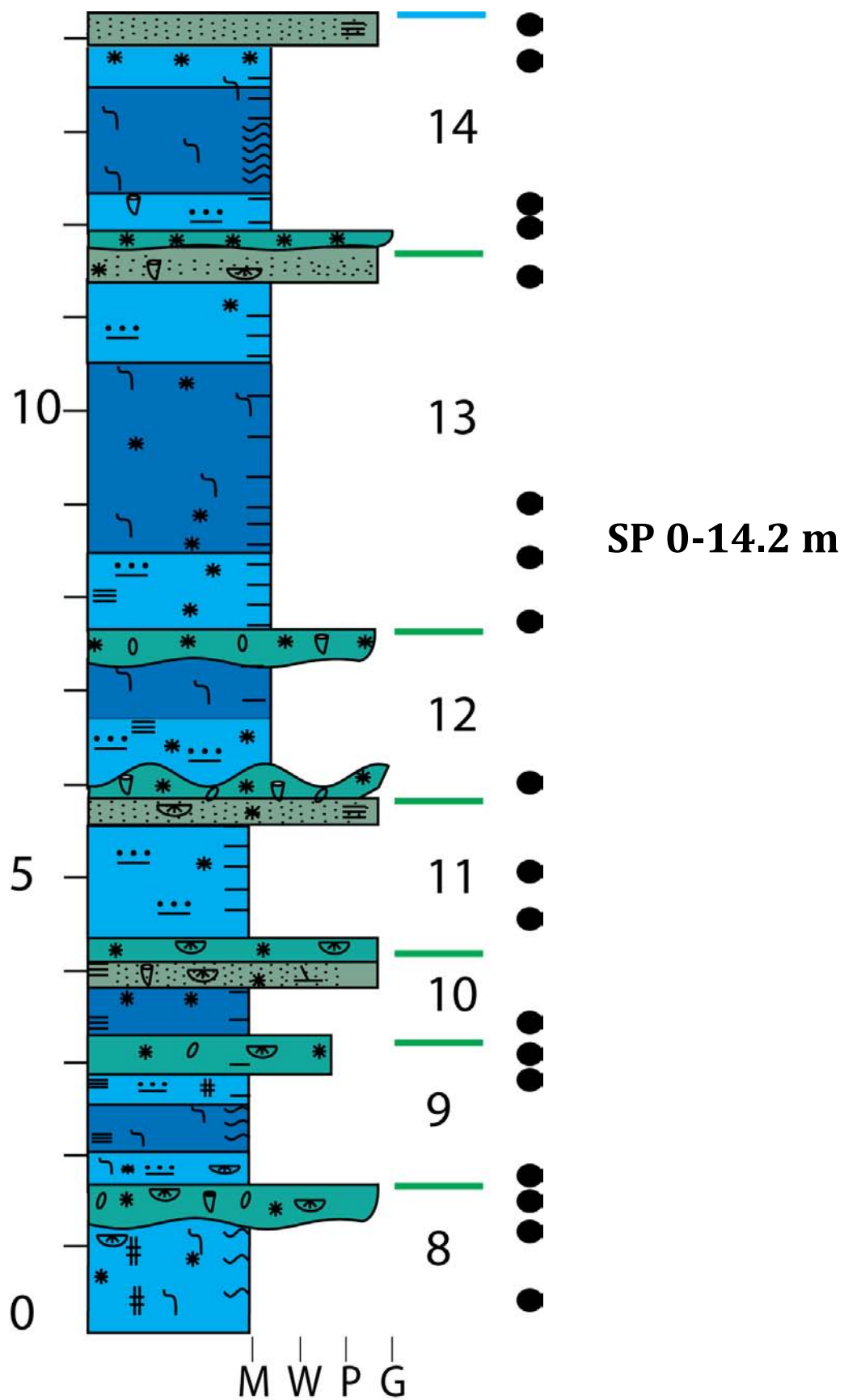
7. APPENDICES

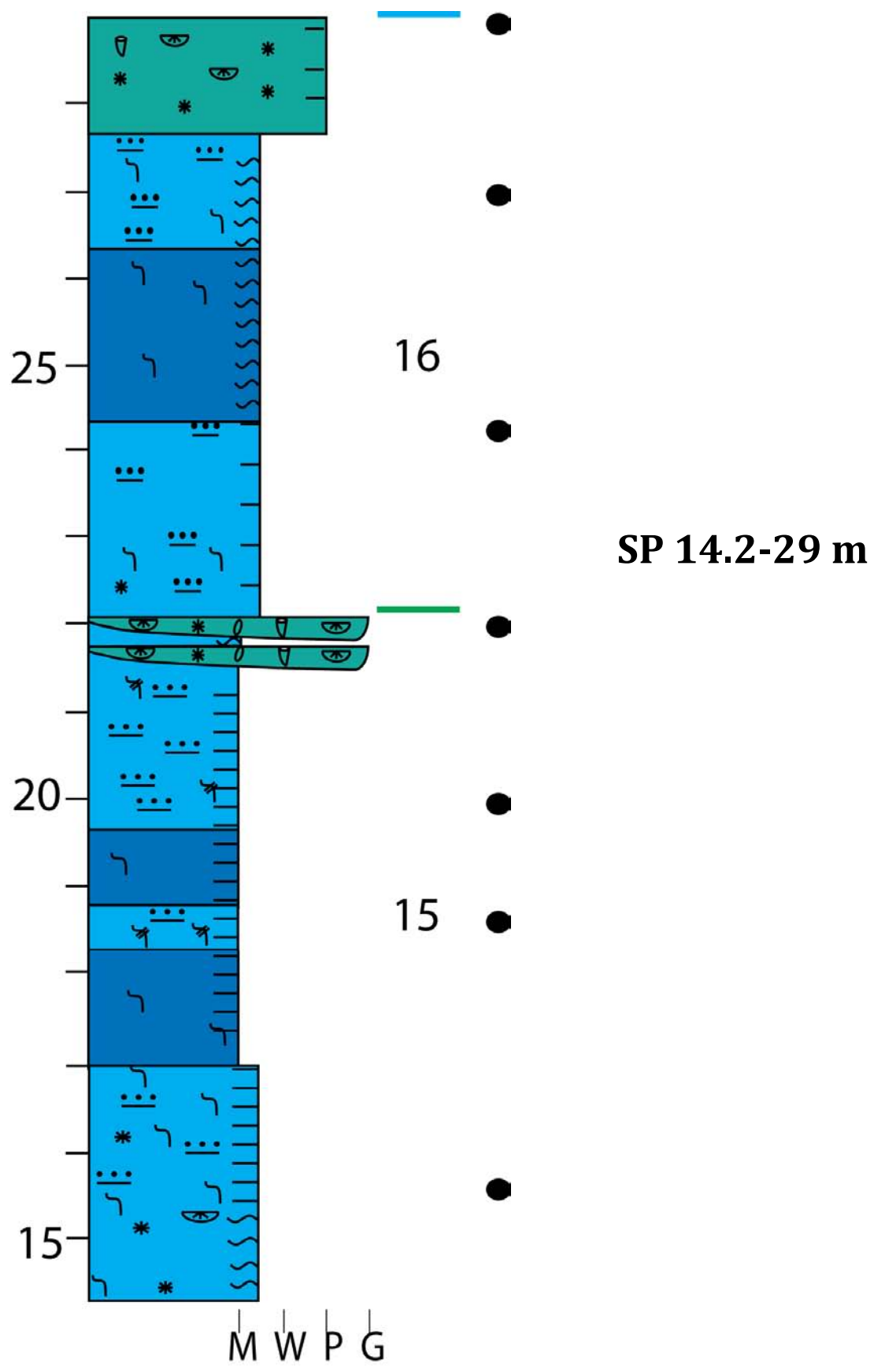
7.1 APPENDIX 1 STRATIGRAPHIC COLUMN

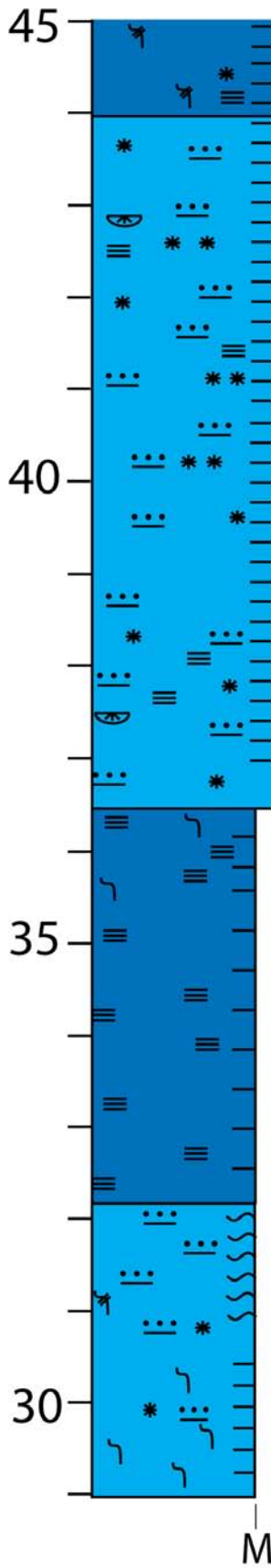
Explanation									
	thin bedded		horizontal burrows		brachiopods		oolitic grainstone		My-scale sequence boundary
	medium bedded		micro scour		rugose coral		peloidal grainstone		intermediate sequence boundary
	nodular bedded		mud drapes		fenestrate bryozoan		crinoidal-pack/grainstone		cycle boundary and number
	laminations		graded bed		coral		graded rhythmites		conodont sample locality
	cross bedding		mud rip-ups		peloids		rhythmites		
	symmetrical ripples		oolitic rip-ups		ooids				
	bioturbation		crinoids						



**SPL (Sacagawea Peak Lower) is the basal 14.2 m of the measured section.
SPL 14.4 lies directly beneath SP (Sacagawea Peak) 0.0 m.**

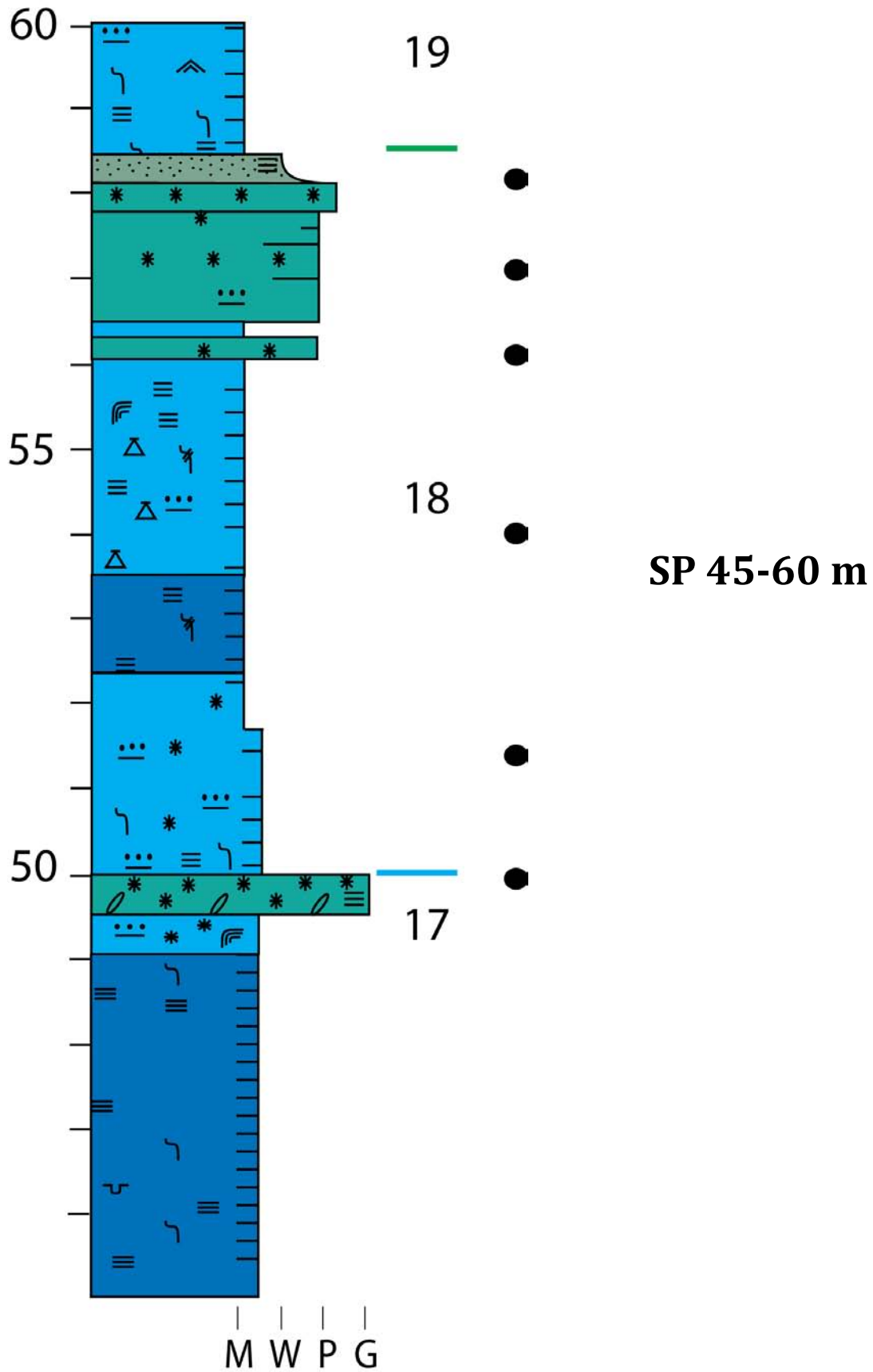


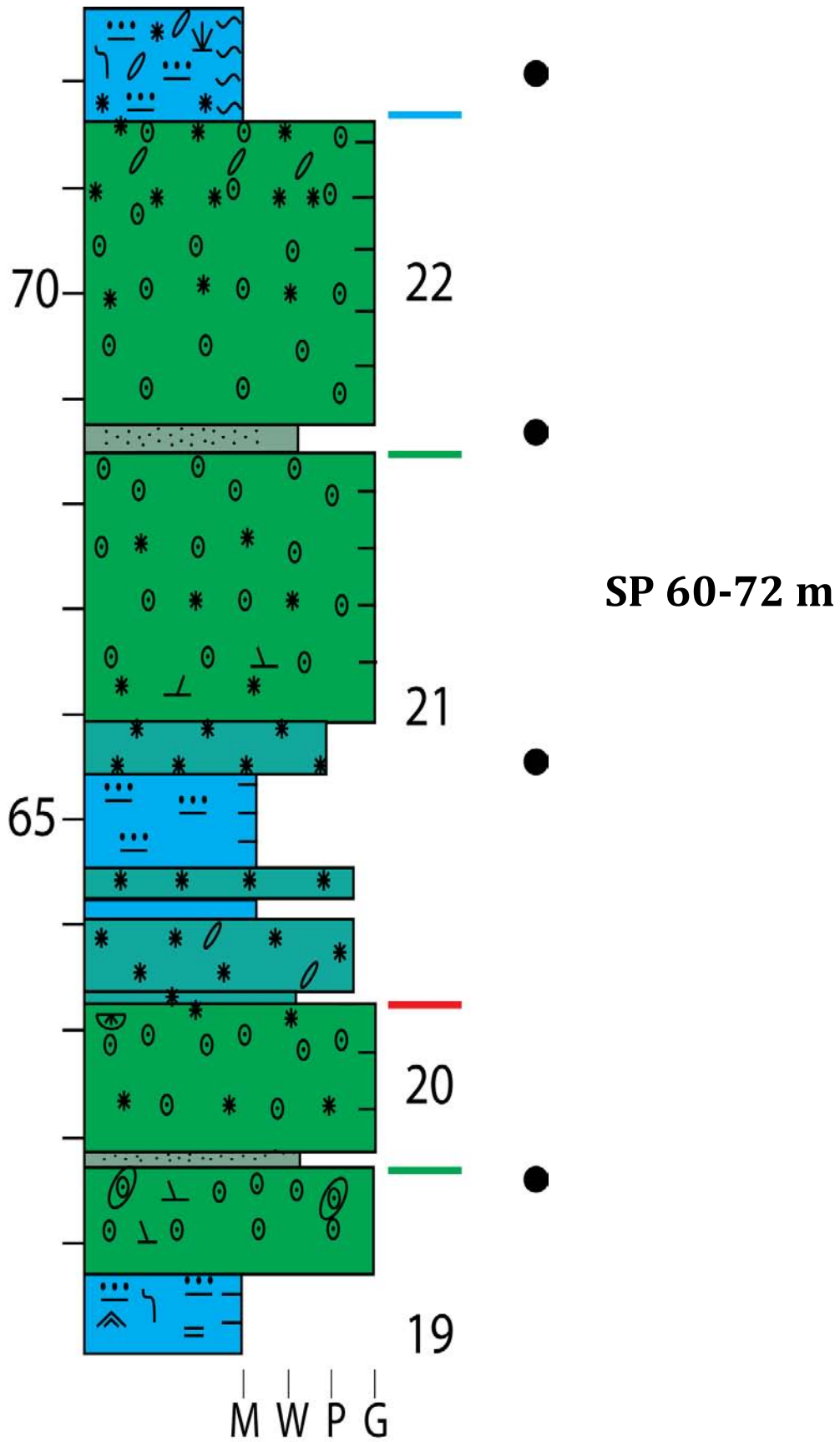




SP 29-45 m







7.2 APPENDIX 2 WHOLE ROCK $\delta^{13}\text{C}_{\text{carb}}$ VALUES

Section	Meter	$\delta^{13}\text{C}_{\text{carb}}$
SP	68	4.89
SP	67.5	4.94
SP	67	5.018
SP	66	4.859
SP	65.5	4.466
SP	65	4.4265
SP	64.5	4.32025
SP	64	4.299
SP	61	4.26475
SP	60.8	4.84725
SP	60.6	4.8185
SP	60.4	4.98475
SP	55.5	5.34225
SP	55	5.433
SP	54.5	5.507
SP	53.5	5.322
SP	53	4.8905
SP	52.5	5.3445
SP	52	5.7135
SP	51.5	5.966
SP	51	5.7525
SP	50.5	5.299
SP	29	6.27475
SP	28.5	6.65575
SP	28	6.51275
SP	27.5	6.625
SP	27	6.403
SP	26.5	6.5865
SP	26	6.0105
SP	25.5	6.40125
SP	24	6.728
SP	23.5	6.8325
SP	23	6.5915
SP	14	6.504
SP	13.8	6.2765
SP	13.5	6.6525
SP	13.1	6.85975

SP	12.9	6.012
SP	12.7	6.6095
SP	12.5	6.5605
SP	12.3	5.5455
SP	12.1	6.6355
SP	10.8	6.6335
SP	10.6	6.9
SP	10.4	7.4905
SP	10.2	6.6045
SP	8.8	6.57225
SP	8.6	6.6065
SP	8.4	7.23575
SP	8.2	5.9375
SP	8	7.18075
SP	7.7	4.354
SP	3.2	6.62
SP	3	7.7613
SP	2.8	5.998
SP	2.6	6.8677
SP	2.4	6.81675
SP	2.2	6.72775
SP	2	7.56
SP	1.6	6.408
SP	1.5	6.218
SP	1.3	5.8355
SP	1	6.52
SP	0.6	6.68075
SP	0.4	6.49575
SP	0.2	6.11325
SP	0	6.509
SPL	14.2	6.044
SPL	13.8	6.4105
SPL	13.6	6.24725
SPL	13.2	6.26375
SPL	12.9	6.26475
SPL	12.7	6.0635
SPL	12.5	6.2385
SPL	11.9	5.83575
SPL	11.7	5.7435
SPL	11.5	5.9655
SPL	10.7	5.85075

SPL	10.5	5.7105
SPL	10.3	4.849
SPL	10.1	5.68025
SPL	8.3	5.93
SPL	8	5.504
SPL	7.8	4.9555
SPL	7.6	5.87775
SPL	7.2	5.58925
SPL	7	5.6115
SPL	6.8	5.42
SPL	6.6	5.56875
SPL	6.4	5.54575
SPL	6.25	5.56975
SPL	1.5	4.68075
SPL	1	5.52525
SPL	0.6	5.337
SPL	0.4	4.942
SPL	0.2	4.7985

7.3 APPENDIX 3 $\delta^{18}O_{\text{apatite}}$ VALUES

SECTION	METER	RUN 1	RUN 2	RUN 3	MEAN
SP	50		20.11		20.11
SP	28.8	19.02			19.02
SP	27	19.01			
SP	27	18.81			18.89
SP	24.3	18.19			
SP	24.3	18.13			18.16
SP	19.9		21		21
SP	18.6		18.6	19.8	
SP	18.6		19.2		19.37
SP	15.6		18.54		18.54
SP	14		19.66		19.66
SP	3	18.37			18.41
SP	3	18.44			
SP	2.8	18.06			18.06
SP	1.7	18.41			18.41
SP	0.4		19.5		19.5
SPL	13.6		20.58		20.58
SPL	11.85		19.66	19.6	19.63
SPL	9.85		20.59	20.1	20.34
SPL	8	21.62			21.62
SPL	7.5	20.88			20.88
SPL	6.6	20.82			20.55
SPL	6.6	20.28			
SPL	6.25	20.1			20.41
SPL	6.25	20.73			
SPL	1.5		19.4		19.4
SPL	1		22.3	19.8	21

REFERENCES

- Aigner, T., 1985, Storm depositional systems, *in* Friedman, G.m., Neugebauer, H.J. and Seilacher, A., eds., *Lecture Notes in Earth Sciences v. 3*: New York, Springer-Verlag, 173 p.
- Beck, J.W., Recy, J., Taylor, F., Edwards, R.L., Cabioch, G., 1997. Abrupt changes in early Holocene tropical sea surface temperature derived from coral records. *Nature* 385, 705–707.
- Blakey, R.C., 2011, Carboniferous-Permian paleogeography of the assembly of Pangaea, <http://jan.ucc.nau.edu/rcb7/globaltext2.html>
- Blanco-Ferrera, S., Sanz-Lopez, J., Garcia-Lopez, S., Bastida, F., and Luz-Valin, M., 2010, Conodont alteration and tectonothermal evolution of a diagenetic unit in the Iberian Variscan belt (Ponga-Cuera unit, NW Spain). *Geology Magazine*, v. 148, p. 35-49.
- Bishop, James W., Montañez, Isabel P., Gulbranson, Erik L., Brenckle, Paul L., The Onset of Mid-Carboniferous Glacio-eustasy: Sedimentologic and Diagenetic Constraints, Arrow Canyon, Nevada, *Palaeogeography* (2009), doi: 10.1016/j.palaeo.2009.02.019
- Bishop, James W., Montanez, Isabel P., and Osleger, D.A., 2010 Dynamic Carboniferous climate change, Arrow Canyon, Nevada, *Geosphere* v. 6, no.1; p.1-34.
- Brezinski, D.K., Cecil, C.B., Skema, V.W., Stamm, R., 2008. Late Devonian glacial deposits from the eastern United States signal an end of the mid-Paleozoic warm period: *Palaeogeography, Palaeoclimatology, Palaeoecology* 268, 143–151.
- Bruckschen, P., and Veizer, J., 1997, Oxygen and carbon isotopic composition of Dinantian brachiopods: paleoenvironmental implications for the Lower Carboniferous of western Europe: *Palaeogeography, Palaeoclimatology, Palaeoecology*, v. 132, p. 243–264.
- Buggisch, W., Joachimski, M.M., Sevastopulo, G., and Morrow, J.R., 2008, Mississippian delta (super 13) and conodont apatite delta (super 18) O records; their relation to the late Palaeozoic glaciation, *Palaeogeography, Palaeoclimatology, Palaeoecology*, v.268, p.273-292.
- Calvet, F., and Tucker, M.E., 1988, Outer ramp cycles in the Upper Muschelkalk of the Catalan basin, northeast Spain: *Sedimentary Geology*, v.

57, p.185-198.

de Wolde, J.R., Bintania, R., Oerlemans, J., 1995. On thermal expansion over the last hundred years

Cecil, C.B., Stamm, R.G., and Skema, V.W., 2002, Evidence for Late Devonian and early Carboniferous global cooling in the Appalachian Basin, Geological Society of American Annual Meeting, Programs with Abstracts v. 34, p.165.

Caputo, M.V., and Crowell, J.C., 1985, Migration of glacial centers across Gondwana during the Paleozoic era: Geological Society of America, Bulletin, v. 96, p. 1020–1036

Chappell, J., Omura, A., Esat, T., McMulloch, M., Pandolfi, J., Ota, Y., Pillans, B., 1996,
Reconciliation of Late Quaternary sea levels derived from coral terraces at Huon Peninsula with deep sea oxygen isotope records: Earth and Planetary Science Letters, v. 141, p. 227-236.

Crowell, J.C., 1983, The recognition of ancient glaciations, Memoir, Geological Society of America, v.161, p.289-297.

Cutler, K.B., Edwards, R.L., Taylor, F.W., Cheng, H., Adkins, J., Gallup, C.D., Cutler, P.M., Burr, G.S., Bloom, A.L., 2003, Rapid sea-level fall and deep-ocean temperature change since the last interglacial period: Earth and Planetary Science Letters, v. 206, p. 253-271.

Cook, H.E., and Taylor, M.E., 1977, Comparison of continental slope and shelf environments in the upper Cambrian and lowest Ordovician of Nevada, *in* Cook, H.E., and Enos, P., eds, Deep-water carbonate environments, Society of Economic Paleontologist Mineralogists, Special Publication, v. 25, p. 51-81.

Elrick, M. and Read, J.F., 1991, Cyclic ramp-to-basin carbonate deposits, Lower Mississippian, Wyoming and Montana, Journal of Sedimentary Petrology, v.61, p.1194-1224.

Elrick, M., Read, J. F., and Coruh, C., 1991, Short-term paleoclimatic fluctuations expressed in Lower Mississippian ramp-slope deposits, southwestern Montana: Geology, 19, 799-802.

Elrick, M. and Hinnov, L.A., 1996, Millennial-scale climate origin for stratification in Cambrian and Devonian deep-water rhythmites, western U.S.A.: Palaeogeography, Palaeoclimatology, Palaeoecology, 123, 353-372.

Elrick, M. and Snider, A. S., 2002, Deep-water stratigraphic cyclicity and carbonate mud mound development in the Middle Cambrian Marjum Formation, House Range, Utah, USA, Sedimentology, 49, 1021-1047.

Elrick, M. and Hinnov, L., 2007, Millennial-scale paleoclimate cycles recorded in widespread Paleozoic deeper water rhythmites of North America, *Palaeogeography, Palaeoclimatology, Palaeoecology*. 243, 348-372.

Elrick., M., Berkyova, S., Klapper, G., Sharp, Z., Joachimski, M., Fryda, J., 2009. Stratigraphic and oxygen isotope evidence for My-scale glaciation driving eustasy in the Early–Middle Devonian greenhouse world, *Palaeogeography, Palaeoclimatology, Palaeoecology*, 276, 170-181.

Epstein, A. G., Epstein, J. B. & Harris, L. D. 1977. Conodont Colour Alteration – an index to organic metamorphism. U.S. Geological Survey Professional Paper 995, p. 1–27.

Fairbanks , R.G. and R.K. Matthews, 1978. The oxygen isotope stratigraphy of the Plesitocene reef tracts of Barbados , West Indies . *Quaternary Research*, 10 (1), 181-196.

Fairbanks, R.G., 1989, A 17,000-year glacio-eustatic sea level record influence of glacial melting rates on the Younger Dryas event and deep-ocean circulation: *Nature*, v. 342, p. 637-642

Fielding, C.R., Frank, T.D., Birgenheier, L.P., Rygel, M.C., Jones, A.T., and Roberts, J., 2008, Stratigraphic imprint of the late Palaeozoic ice age in eastern Australia: A record of alternating glacial and non- glacial climate regime: *Geological Society of London Journal*, v. 165, p. 129–140, doi: 10.1144/ 0016-76492007-036.

Frakes, L.A., Francis, J.E., and Syktus, J.I., 1992, *Climate modes of the Phanerozoic*, Cambridge University Press, 274 pp.

Goldhammer, R.K., Lehmann, P.J., and Dunn, P.A., 1993, The origin of high-frequency platform carbonate cycles and third-order sequences (Lower Ordovician El Paso Gp, West Texas): constraints from outcrop data and stratigraphic modeling, *Journal of Sedimentary Petrology*, v.63, p.318-359.

Gonzalez, C.R., 2001, New data on the Late Palaeozoic glaciations in Argentina: *Newsletter on Carboniferous Stratigraphy*, v. 19, p. 44–45.

Gutschick, R.C., Sandberg, C.A., and Sando, W.J., 1980, Mississippian shelf margin and carbonate platforms from Montana to Nevada, *in* Fouch, T.D., and Magathan, e.R., eds., *Rocky Mountains Section SEPM Paleozoic Paleogeography of the West-Central United States*, Rocky Mountain Paleogeography Symposium 1, p. 111-128.

Gradstein, F.M., Ogg, J.G., Smith, A.G., Agterberg, F.P., Bleeker, W., Cooper, R.A., Davydov, V., Gibbard, P., Hinnov, L.A., House, M.R., Lourens, L., Luterbacher, H.P., McArthur, J., Melchin, M.J., Robb, L.J., Shergold, J., Villeneuve, M., Wardlaw, B.R., Ali, J., Brinkhuis, H., Hilgen, F.J., Hooker, J., Howarth, R.J., Knoll, A.H., Laskar, J., Monechi, S., Plumb, K.A., Powell, J., Raffi, I., Röhl, U., Sadler, P., Sanfilippo, A., Schmitz, B., Shackleton, N.J., Shields, G.A., Strauss, H., Van Dam, J., van Kolfschoten, T., Veizer, J., Wilson, D., 2004. A Geologic Time Scale 2004. Cambridge University Press, p. 589.

Hagan, G.M., and Logan, b .W., 1974, Development of carbonate banks and hypersaline basins, Shark Bay, Western Australia, *in* Evolution and Diagenesis of Quaternary Carbonate Sequences, Shark bay, Western Australia: American Association of Petroleum Geologists Memoir 22, p. 61-139.

Hambrey, M.J., and Harland, W.B., 1981, Earth's pre-Pleistocene glacial record (ed.) Chumakov, N.M., Fancett, K.E., Herod, K.N. and Wang Zejiu, Cambridge University Press, Cambridge, United Kingdom, 1019pp.

Handford, C.R., 1986, Facies and bedding sequences in shelf-storm-deposited carbonates; Fayetteville Shale and Pitkin Limestone (Mississippian), Arkansas: *Journal of Sedimentary Petrology*, v. 56, p. 123-137.

Heckel, P.H., 1994, Evaluation of evidence for glacial-eustatic control over marine Pennsylvanian cyclothems in North America and consideration of possible tectonic effects, *in* Denison, J.M., and Etensohn, F.R., eds., Tectonic and eustatic controls on sedimentary cycles: Concepts in Sedimentology and Paleontology, v. 4, p. 65–87.

Horbury, A.D., 1989, The relative role of tectonism and eustasy in the deposition of the Urswick Limestone in South Cumbria and North Lancashire, *in* Arthurton, R.S., Gutteridge, P, and Nolan, S.C. eds. The role of tectonics in Devonian and Carboniferous sedimentation in the British Isles. Yorkshire geological Society. Occasional Publications, v. 6, p. 153-169.

Huneke, H., Joachimski, M., Buggisch, W., and Lutzner, H., 2001, Marine carbonate facies; *in*, Response to Climate and Nutrient Level—The Upper Carboniferous and Permian of Central Spitsbergen (Svalbard): Facies, v. 45, p. 93-136.

Isbell, J.L., Miller, M.F., Wolfe, K.L., and Lenaker, P.A., 2003, Timing of the late Paleozoic glaciation in Gondwana: was glaciations responsible for the development of Northern Hemisphere cyclothems?, Special Paper, Geological Society of America, v.370, p.5-24.

Joachimski, M.M., von Bitter, P.H., Buggisch, W., 2006. Constraints on Pennsylvanian glacioeustatic sea-level changes using oxygen isotopes of conodont apatite. *Geology* 34, 277–280.

- Katz, D.A., et al., Timing and local perturbations to the carbon pool in the lower Mississippian Madison Limestone, Montana and Wyoming, *Palaeogeography, Palaeoclimatology, Palaeoecology* (2007), doi:10.1016/j.palaeo.2007.02.048
- Lehrmann, D.J., Goldhammer, R.K., 1999. Secular variation in facies and parasequence stacking patterns of platform carbonates: a guide to application of the stacking patterns technique in strata of diverse ages and settings. In: Harris, P.M., et al. (Ed.), *Recent Advances in carbonate sequence stratigraphy; applications to reservoirs, outcrops and models*: SEPM, Society for Sedimentary Geology, Special Publication, vol. 63, pp. 187–226.
- Linsley, B. K., and R. B. Dunbar, 2003, The late Pleistocene history of surface water $\delta^{13}\text{C}$ in the Sulu Sea: Possible relationship to Pacific deep water $\delta^{13}\text{C}$ changes, *Paleoceanography*, v 9, p 317–340.
- Lisicki, L.E. and Raymo, M.E.A. 2005, Pliocene-Pleistocene stack of 57 globally distributed $\delta^{18}\text{O}$ records, *Paleoceanography* 20.
- Lloyd, R.M., Perkins, R.D., and Derr, S.d., 1987, Beach and shoreface ooid deposition on shallow interior banks, Turks and Caicos islands, British West Indies: *Journal of Sedimentary Petrology*, v. 67, p.976-982.
- Loreau, J.P., and Purser, B.H., 1973, Distribution of ultrastructure of Holocene ooids in the Persian Gulf, *in* Purser, B.H., ed., *The Persian Gulf*: New York, Springer-Verlag, p. 279-328.
- Matchen, D.L., and Kammer, T.W., 2006, Incised valley fill interpretation for Mississippian Black Hand Sandstone, Appalachian Basin, USA: implications for glacial eustasy at Kinderhookian–Osagean (Tn2–Tn3) boundary: *Sedimentary Geology*, v. 191, p. 89–113
- Markello, J.R., and Read, J.f., 1982, Upper Cambrian intrashelf basin, Nolichucky Formation, southwest Virginia Appalachians: *American Association of Petroleum Geologists Bulletin*, v. 66, p. 860-878.
- Mii, H.S., Grossman, E.L., Yancey, T.E., 1999. Carboniferous isotope stratigraphies of North America: implications for Carboniferous paleoceanography and Mississippian glaciation. *Geological Society of America Bulletin* 111, 960–973.
- Mix, A.C., 1987. The oxygen-isotope record of glaciation. In: *North America and Adjacent Oceans During the Last Deglaciation, the Geology of North America v.K-3*, eds. Ruddiman W.f., and Wright, H.E., Boulder: Geological society of America p. 111-135.

Mix, A.C., Pisias, N.G., Rugh, W., Wilson, J., Morey, A., and Hagelberg., 1995, Benthic foraminifer stable isotope record from site 849 (0-5 Ma): local and global climate changes *in* Pisias, N.g., Mayer, L. A., Janecek, T. R., Palmer-Julson, A., and van Andel, T.H., eds. Proceedings of the ocean Drilling Program, Scientific Results, v. 138, p. 371-412.

Mohseni, H. and Al-Aasm, S. 2004. Tempestite deposits on a storm-influenced carbonate ramp: An example from the Pabdeh Formation (plaleogene), Zagros basin, SWIran. *Journal of Petroleum Geology*, Vol.27, No.2.

Nöth, S. 1998. Conodont color (CAI) versus microcrystal- line and textural changes in Upper Triassic conodonts from Northwest Germany. *Facies* 38, p. 165–74.

O'Neil, J.R., Roe, L.J., Reinhard, E., Blacke, R.E., 1994. A rapid and precise method of oxygen isotope analysis of biogenic phosphate. *Israel Journal of Earth Science* 43, 203–212.

D.W. Oppo, M.E. Raymo, G.P. Lohmann, A.C. Mix, J.D. Wright and W.L. Prell , A, 1995, $\delta^{13}\text{C}$ record of upper North Atlantic Deep Water during the last 2.6 million years. *Paleoceanography* **10** (1995), pp. 373–394.

Osleger, D, A., 1991, Subtidal carbonate cycles: implications for allocyclic versus autocyclic controls: *Geology*, v. 19, p. 917-920.

Oslegar, D.A., and Read, J.F., 1991, Relation of eustasy to stacking patterns of meter-scale carbonate cycles, Late Cambrian, USA. *Journal of Sedimentary Petrology*, v. 61, p. 1225-1252.

Pekar, S., Christie-Blick, N., Kominz, M.A., Miller, K.G., 2002. Calibration between eustatic estimates from backstripping and oxygen isotope records for the Oligocene. *Geology* 30, 903–906.

Pekar, S., Hucks, A., Fuller, M., Li, S., 2005. Glacioeustatic changes in the early and middle Eocene (51–42 Ma): shallow-water stratigraphy from ODP Leg 189 Site 1171 (South Tasman Rise) and deep-sea delta 0-18 records. *Geological Society of American Bulletin* 117, 1081–1093.

Poole, F.G., and Sandber, C.A., 1977, Mississippian paleogeography and tectonics of the Western United States, *in* Peterson, J.A., ed., *Paleotectonics and Sedimentation in the Rocky Mountain Region, U.S.*: American Association of Petroleum Geologists Memoir 41, p. 3-19.

Puceat, E., Joachimski, M. M., Bouilloux, A., Monna, F., Motreuil, P., Henard, S., Mourin, J., Dera, G., and Quesne, D., 2010, Revised phosphate-water

- fractionation equation reassessing paleotemperatures derived from biogenic apatite: *Earth and Planetary Science Letters*, v. 298, p. 135-142.
- Read, J.F., 1980, Carbonate ramp-to-basin transitions and foreland basin evolution, Middle Ordovician, Virginia Appalachians: *American Association of Petroleum Geologists Bulletin*, v. 64, p. 1575-1612.
- Read, J.F., Kerans, C., Weber, L.J., Sarg, J.F., and Wright, F.M., 1995, Milankovitch Sea-Level Changes, Cycles and Reservoirs on Carbonate Platforms in Greenhouse and Icehouse Worlds:, *SEPM, Short Course Notes 35*, 81 pp.
- Ross, C.A., and Ross, J.R.P., 1985, Late Paleozoic depositional sequences are synchronous and worldwide: *Geology*, v. 13, p. 194–197.
- Ruddiman, W.F., 2002. *Earth's Climate Change: Past and Future*. Freeman, New York. 465 pp.
- Sando, W.J., 1976, Mississippian history of the northern Rocky Mountains region: *Journal of Research, U.S. Geological Survey*, v. 4, p. 317-338.
- Sando, W.J., 1985, Revised Mississippian time scale, western interior region, conterminous United States: *U.S. Geological Survey Bulletin 160-5A*, p A15-A26.
- Spotl, C. and Vennemann, T. W. 2003 Continuous-flow isotope ratio mass spectrometric analysis of carbonate minerals. *Rapid Communications In Mass Spectrometry* v. 17, n 9, p. 1004-1006
- Saltzman, M.R., 2002, Carbon and oxygen isotope stratigraphy of the Lower Mississippian (Kinderhookian-lower Osagean), western United States: Implications for seawater chemistry and glaciation, *GSA Bulletin*, v. 114, p. 96-108.
- Saltzman, M.R., Gonzalez, L.A., Lohmann, K.C., 2000a. Earliest Carboniferous cooling step triggered by the Antler Orogeny? *Geology* v. 28, p. 347–350.
- Saltzman, M.R., Groessens, E., and Zhuravlev A.V., 2004, Carbon cycle models based on extreme changes in $\delta^{13}C$: an example from the lower Mississippian, *Paleogeography*, v.213, p. 359-377. doi:10.1016/j.palaeo.2004.07.01
- Soreghan, G.S., and Giles, K.A., 1999, Amplitudes of late Pennsylvanian glacioeustasy: *Geology*, v. 27, p. 255–258.
- Smith, L.B., JR., and Read, J.F., 1999, Application of high-resolution sequence stratigraphy to tidally influenced upper Mississippian carbonates, Illinois Basin, in Harris, P.M., Saller, A.H., and Simo, J.A., eds., *Advances in Carbonate*

Sequence Stratigraphy: Application to Reservoirs, Outcrops and Models: SEPM, Special Publication 63, p. 107–126.

Smith, L.B., and Read, J.F., 2000, Rapid onset of late Paleozoic glaciation on Gondwana: evidence from upper Mississippian strata of the midcontinent, United States: *Geology*, v. 28, p. 279–282.

Sonnenfeld, M. D., 1996, Sequence evolution and hierarchy within the lower Mississippian Madison Limestone of Wyoming, in M. W. Longman and M. D. Sonnenfeld, eds., *Paleozoic systems of the Rocky Mountain region: Rocky Mountain Section*, SEPM, p. 165–192.

Speed, R.C., and Sleep, N.H., 1982, Antler orogeny and foreland basin: a model: *Geological Society of America Bulletin*, v. 93, p. 815-828

Sweet, A.G., and Harris, W.C., 1989, Mechanical and chemical techniques for separating microfossils from rock, sediment, and residue matrix, *Special Publication*, Paleontological Society, v.4, p.70-86.

Tucker, M. E., and V. P. Wright. 1990. *Carbonate sedimentology*. Blackwell Science, 482 p.

Veevers, J.J., and Powell, McA.C., 1987, Late Paleozoic glacial episodes in Gondwanaland reflected in transgressive-regressive depositional sequences in Euramerica: *Geological Society of America Bulletin*, v. 98, p. 475-487.

Vennemann, T.W., Fricke, H.C., Blake, R.E., O'Neil, J.R., Colman, A., 2002. Oxygen isotope analysis of phosphates: a comparison of techniques for analysis of Ag_3PO_4 . *Chemical Geology* 185, 321–336.

de Wolde, J.R., Bintania, R., Oerlemans, J., 1995. On thermal expansion over the last hundred years. *Journal of Climate* 8, 2881–2891

Wright, V.P., and Vanstone, S.D., 2001, Onset of late Palaeozoic glacio-eustasy and the evolving climates of low latitude areas: a synthesis of current understanding: *Geological Society of London, Journal*, v. 158, p. 579–582.